A QUANTITATIVE ANALYSIS OF INTERSTITIAL FLUID CHEMISTRY AND LIMESTONE DISSOLUTION RATES WITHIN THE CLASTIC SEDIMENT OF A KARST AQUIFER CONDUIT, MAMMOTH CAVE, KENTUCKY

A Thesis
Presented to
the Faculty of the Department of Geography and Geology
Western Kentucky University
Bowling Green, Kentucky

In Partial Fulfillment
of the Requirements for the Degree of
Master of Science in Geography

by
Kevin Benjamin Vaughan
December 1998

A QUANTITATIVE ANALYSIS OF INTERSTITIAL FLUID CHEMISTRY AND LIMESTONE DISSOLUTION RATE WITHIN THE CLASTIC SEDIMENT OF KARST AQUIFER CONDUIT, MAMMOTH CAVE, KENTUCKY

Date of Recommended Oct 16, 1998

Christopher G. Groves
Director of Thesis

Nicholas C. Crawford

Kenneth W. Kuehn

Edmund Sonn 1-25-99
Dean, Graduate Studies and Research Date

ACKNOWLEDGMENTS

There are many people who have dedicated many hours of their valuable time, and without their tireless efforts I would not have been able to complete this thesis. I would like to mention several individuals by saying thank you. Dear Dr. Chris Groves my thesis advisor, I cannot begin to express my gratitude, and my appreciation for the insightful comments, and the well deserved criticisms. Not only do I thank you regarding the direction of my thesis but also the effort and heart warming affection that you expressed towards my whole family. Without that sincere friendship I probably would have left Bowling Green soon after I had arrived. I would also like to thank my thesis committee members, Dr. K. Kuehn, Dr. N. Crawford, Dr. C. Moore, and J. Meiman, who devoted their time, energy, and creative thoughts towards the improvement of my thesis.

To my wife: Dear Nicole without your understanding, patience, and encouragement I would have given up on graduate school at least 1000 times. Not only do I appreciate your moral support and encouragement but I also thank you for the time and energy that you dedicated towards my thesis.

I give special thanks and acknowledgments to many others who have made this thesis possible by giving me helpful discussion, comments, criticism, time, and energy: D. Anthony, D. Carigan, Dr. B. Madison, Dr. M. May, Dr. E. McClellan, D. Kreizer, Dr. D. Kuehn, and A Vaughan. I give additional thanks to the administration at Mammoth Cave National Park who allowed my research to proceed within their protected area. I gratefully acknowledge financial support from Western Kentucky University, and the National Speleological Society.

TABLE OF CONTENTS

LIST OF FIGURES

LIST OF TABLES

ABSTRACT

Many active stream conduits within karst aquifers transport and deposit non-carbonate, clastic sediment. However, little is known about how these sediments impact conduit development and enlargement rates. For example, can dissolution take place at the sediment/bedrock interface beneath a flowing stream? If not, cavern enlargement might be dominated by flood conditions when the bare rock of the walls and ceiling are in contact with the dissolving fluids.

An approach using limestone tablet weight loss experiments, along with water sampling and geochemical modeling, has been undertaken to understand the nature of fluid movement and chemistry with the sediment beneath an active flowing cave stream within the Kentucky's Mammoth Cave System. Fluid flow and carbonate chemistry were compared between the active stream and within the sediment at 15, 30, 60, and 90 cm below the stream bed. It was found that carbon dioxide pressure within the interstitial fluids was elevated an order of magnitude above that of the stream waters, having levels as much as 31 times that of atmospheric background, presumably from microbial decomposition of organic material. The fluids were all undersaturated with respect to calcite (SI= -0.4 to -0.9), and limestone blocks buried at these levels all dissolved (rates from 0.8 to 21.9 g m -2 yr -1). These results suggest that at some locations the limestone bedrock may be dissolving beneath clastic sediment deposits; which in turn has implications for understanding rates and geometries of conduit evolution within karst aquifers.

CHAPTER I

INTRODUCTION AND GENERAL CONCEPTS

Introduction

Although significant progress has been made in understanding cave development in limestone, the details of the small-scale interactions that control cave-forming processes require more study. For example, does passage development occur only along the ceiling, floor, or both directions, and what impact does abrasion have on conduit development? A significant amount of research has been undertaken in the south-central Kentucky karst area which is one of the better places in the world for study of karst landscapes and the mechanisms by which they form. There are several reasons why the previous statement is true: (1) cave passages within the region are extremely extensive, with a current surveyed length of approximately 800 km lying within an area of about 250 km^2 which also includes the Mammoth Cave system presently mapped at 500+ km, (2) the Mammoth Cave system has well-developed cave passages, with relatively easy access, (3) comprehensive maps have been created from the years of extensive exploration and survey, and (4) detailed geological, geochemical, and hydrological studies have been made of the area.

Caves are the voids that remain after portions of the carbonate bedrock, most

commonly limestone, have been removed through dissolution by flowing groundwater. Within the Mammoth Cave area the most important dissolution reactions is that of carbonic acid (H_2CO_3) (White, 1988).

Dissolution of limestone by water flowing through the aquifer has formed several different types of cave passages within the Mammoth Cave area. Cave passages may display an elliptical shape, a tall and narrow "canyon" shape, or a keyhole-shaped cross section formed from a combination of the previous two types (Figure 1).

The distinctive cross-sectional shapes of cave passages reflect the hydrologic conditions under which they formed. Elliptical passages form below the water table where the conduits are completely filled. Under these conditions water is in contact with the entire passage cross section, and dissolution proceeds outward in almost all directions. Canyon passages, in contrast, may form in several different ways. The most common process in the south-central Kentucky karst appears to be the mechanism of vadose entrenchment. Vadose entrenchment suggests that continuous downward dissolution occurs on the cave floor, resulting in a tall, narrow shape. An alternative idea for canyon development, suggested by Renault (1970) and Ford and Ewers (1978), is known as paragenesis. Paragenesis suggests that limestone dissolution will not occur in parts of cave passages that are covered with clastic sediment, which inhibits dissolution. Therefore, the passage must form upwards during periods when the walls and ceiling are in contact with dissolving fluids.

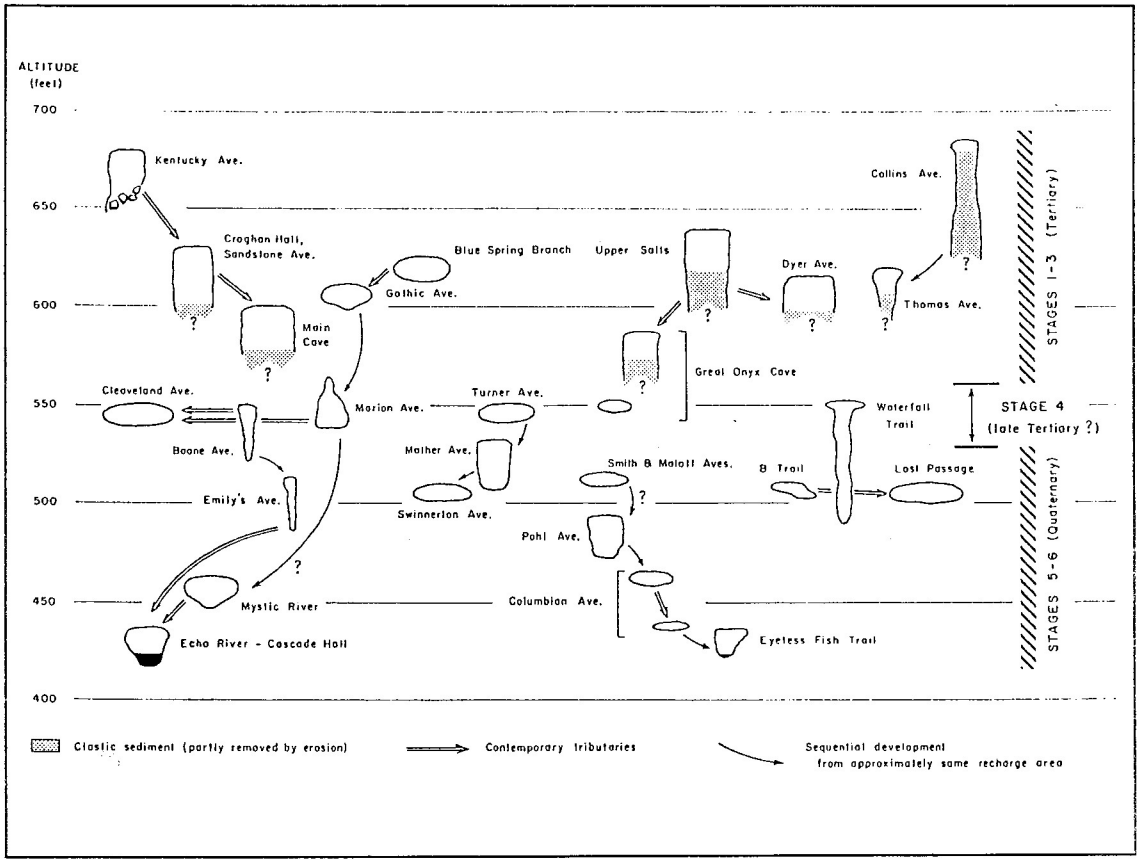

Figure 1. Different passage shapes at Mammoth Cave National Park (Source: Palmer, 1989).

Theories of cave passage development

For the past thirty years, the processes that form different passage types have been greatly debated. Within the Mammoth Cave area there are three main types of passages: elliptical, keyhole-shaped, and rectangular canyon passages. The elliptical passages are known as phreatic tubes. Within the Mammoth Cave area the elliptical pipes are remarkably uniform with the long axis of the ellipse parallel to bedding (White and Deike, 1989). The keyhole passages are formed from the combination of the elliptical and

canyon passage.

Many cave passages within the Mammoth Cave area are tall, narrow and partly filled with sediment. There are two schools of thought on the development of tall and narrow cave passages within the Mammoth Cave area: (1) paragenesis, and (2) vadose entrenchment.

Paragenesis

The idea of paragenesis states that cave passage development can only occur in phreatic (when the entire passage is beneath the water table) conditions that will allow limestone dissolution within the passage to occur exclusively in an upward direction. This phenomenon occurs as a result of sediment deposition along the floor and walls of caves passages which, in theory, acts as an inhibitor toward further limestone dissolution. Through time as the passage enlarges upward, more sediment is deposited on the floor and, as a result, the average flow velocity remains rather constant at the threshold of sediment transport (Palmer, 1989). In extreme cases, a high canyon might be produced entirely in the phreatic zone, with upward solution terminating only at the water table (Ford and Ewers, 1978). The results are tall and narrow caves that are mostly filled with clastic sediment.

Vadose entrenchment

The vadose entrenchment theory, as noted previously, states that there is

continuous limestone dissolution along the stream bed, resulting in a constant downward growth of the cave passage. The results from vadose entrenchment can be tall, narrow cave passages that may later become filled with sediment (Figure 2). Palmer (1989) stated that paragenesis is a compelling prospect for the origin of levels A and B (the uppermost passages) within the Mammoth Cave System because a paragenetic passage requires only a single phase of development. Moreover, deposits caused by a rapid rise in base level can be scattered unless the rise in base level is slow and uniform and the passages are large enough to allow the flow velocity to fall below the critical tractive force. According to Palmer (1989), sediment in most caves is rarely the product of either aggradation or paragenesis. It accumulates mainly as sand and gravel in active stream passages and as clay and silt in areas of rather static flooding. Collapse or similar blockage can cause local filling of a passage with sediment, which gives evidence that canyons within the Mammoth Cave System are not paragenetic.

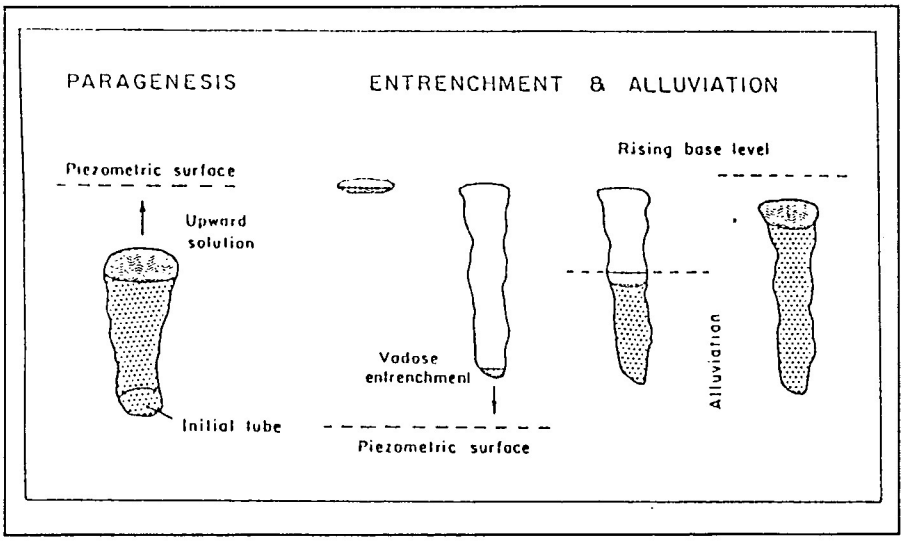

Figure 2. Paragenesis and vadose entrenchment (Source: Palmer, 1989).

Palmer (1989) gave the following evidence from the Mammoth Cave area that argues in favor of vadose entrenchment and aggradation as the result of a fluctuating base level:

1) Many passages are filled to the ceiling with sediment.

2) Cut-and-fill structures and sinuous channels in the sediment suggest open-channel flow.

3) The ceilings of all passages in level B and most of Collins Avenue (level A) are perfectly concordant with the strata, implying that the initial solution took place at those horizons.

4) Breakdown blocks identified stratigraphically occur in the sediment as much as 7 meters below their points of origin, indicating rather large passage heights at the time of breakdown.

5) Some sediment-filled passages in level B are wide, low, sediment-filled tubes rather than canyons.

(6) Known phreatic loops in Mammoth Cave contain only scattered, thin, irregular deposits with little upward solution above them.

Even though some researchers believe that paragenesis is not responsible for the development of cave passages within the Mammoth Cave area, the question has not been quantitatively studied or fully answered. There is substantial evidence in favor of vadose entrenchment within the Mammoth Cave area. Yet, only a gradual rise in base level or paragenesis can account for the tens of meters of stratified sand and gravel observed in levels A and B of Mammoth Cave (Palmer, 1989). Palmer (1989) also stated that paragenetic canyons could easily be mistaken for vadose canyons that have been partly filled with sediment.

Sediments transported into cave passages may coat the floors and walls of those passages, and potentially act as an inhibitor towards further dissolution in the covered areas. Sediments can be transported into cave passages by several different means. Sediments within the Mammoth Cave area are transported predominately by fluvial processes, sinking streams and soil infiltration. An increase in precipitation generally increases the velocity of water flowing within cave passages, which increases the amount of sediment being transported. After the rain ceases, the water velocity decreases, and so does the amount of sediment that can be transported.

According to White (1988) and measurements by Davies and Chao (1959), Mammoth Cave passages are filled with sediment that exhibit a complex stratigraphy of interbedded sands, gravels, cobbles, silt, and clays. Silt was the predominant clastic size particle found in most cave passages, while true clays were rarely found expect near the top of some sediment piles. They did not test whether or not the sediment beds have an effect on dissolution rates of limestone beneath them. In order to understand how these tall and narrow cave passages have formed it is necessary to determine what happens beneath the sediment where the interstitial water comes in contact with the limestone surface. However, the idea that the clastic sediment, covering the floors of many limestone caves inhibits dissolution (upon which paragenesis is based) has not been quantitatively studied.

It is important to decide between the theories of paragenesis and vadose entrenchment because the geomorphic and hydrologic implications of these two possible

origins are radically different (Palmer, 1989). Determination of whether or not clastic sediment has an impact on limestone dissolution rates will add in our understanding cave passage development at the bedrock/sediment interface and will shed light on the current debate between paragenesis and vadose entrenchment. A better understanding of cave passage development will aid in modeling and predicting past and future behavior of karst aquifers. It will also help us understand the hydrologic evolution of the complex Mammoth Cave system.

The clastic sediment found along the floor and walls of a cavern passage is known as weathering detritus. The source of weathering detritus in caves is from the residual soils on the land surface and is generally transported by sinkholes and sinking streams (White, 1988). Sediment within Mammoth Cave also derives from the mechanical and chemical breakdown of the sandstone caprock (White, 1988). A smaller amount comes from an insoluble residue from limestone weathering. Sediment is introduced into and transported within the Mammoth Cave aquifer by water flowing within fractures and conduits. An abundance of deposited gravel, sand, and silt can be found along the floor and walls of Mammoth Cave passages, but clay particles comprise only a small amount of the total sediment (White, 1988).

Ongoing research (Groves and Meiman, 1996) suggests that the dissolution of the major active conduits within the Mammoth Cave aquifer may take place during times when the cave passages are filled to the ceiling with water as a result of storms. It has not been determined, however, how the clastic sediment commonly armoring the floors

of these passages affects limestone dissolution. In addition, a small amount of organic matter can be found within the sediment in many of the aquifer's major base level subsurface passages. In many areas, greater than ten percent of the sediment is composed of organic matter. If the organic matter within the sediment still has a sufficient amount of nutrients available, microbial decomposition of the organic matter may release CO_2, resulting in an increase of Pco_2 (partial pressure of carbon dioxide) and a decrease in the pH causing the groundwater to become more undersaturated with respect to calcite, the predominant mineral of limestone.

Research questions

How have the complex passages within the Mammoth Cave area formed? Paragenesis assumes that the non-carbonate sediment will protect portions of a cave passage, mainly the floor, from the dissolving fluids. Current research within an active conduit in the Mammoth Cave area provides evidence the predominate passage development occurs when the conduit is filled with dissolving fluids, but this research does not consider the impact that the non-carbonate sediment has on passage development.

In this study the purpose is to investigate the following questions. (1) What impact does the clastic sediment have on limestone dissolution rates at the sediment-bedrock interface? (2) How does the clastic sediment affect passage development?

CHAPTER II

THE STUDY AREA

Location

This study of the hydrologic and geochemical behavior of interstitial fluids within karst aquifer river sediments was undertaken within Mammoth Cave National Park (MCNP), which is part of the south-central Kentucky karst (Figure 3). The south-central Kentucky karst is part of a karstic limestone belt that extends from southern Indiana through Kentucky into Tennessee west of the Cumberland River, and along the entire eastern and southern perimeters of the Western Kentucky Coal Field. South-central Kentucky karst is a world renowned example of a shallow, intensely karstified, carbonate landscaped aquifer system (Hess *et al.*, 1989).

Southeast of the Mammoth Cave National Park is the Pennyroyal Plateau, upon which an extensive and well developed Sinkhole Plain has formed. Towards the northwest is the Chester Upland which is part of the Western Kentucky Coal Field. The edge of the Mammoth Cave Plateau forms an escarpment known locally as the Dripping Springs Escarpment, and forms the scarp slope of a cuesta defining the eastern rim of the Illinois Interior Basin. The Pennyroyal Plateau is subdivided into two areas: the Sinkhole Plain, a band characterized by thousands of sinkholes and little surface drainage, and the Glasgow Upland, an area of largely surface drainage. Many of the streams draining the

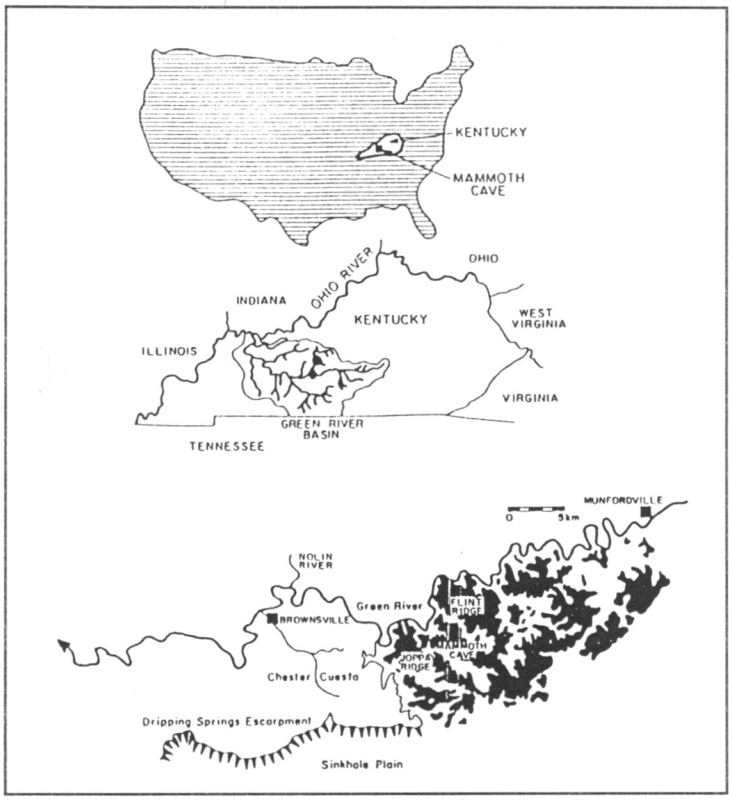

Figure 3. Location map for the Mammoth Cave area and the south-central Kentucky karst (Source: White, 1989).

the Glasgow Upland sink underground as they meet the Sinkhole Plain, forming a boundary between the two (Quinlan and Ray, 1989).

The Mammoth Cave karst aquifer of south-central Kentucky has developed within Meramec and lowest Chester strata of Mississippian age limestone, approximately 160 meters in thickness. The limestone in the area is a world-class example of a shallow, well developed karst landscape through which the majority of the groundwater flows by way of a highly integrated complex conduit system. The limestone in this area has an average dip to the northwest of 6m/km and is exposed along the flank between the

Cincinnati Arch, a wide anticlinal fold that extends from the northeastern Lexington Dome to the southwestern Nashville Dome, and the southeastern edge of the Illinois Basin onto which local, gentle structures are superimposed (Hess, 1976).

Boundaries of the south-central Kentucky karst occur at the region's major surface streams. These boundaries on the south and southwest are fixed by the Barren River, on the south by Beaver Creek, on the east by Little Barren River and Lynn Camp Creek, on the north by Bacon Creek, and on the northwest by the Nolin and Green River (Quinlan and Ewers, 1981). This region is composed of 2,100 km^2 south of the Green River and 600 km^2 north of the river.

The oldest rocks in the karst area belong to the Salem, and Harrodsburg Warsaw Formations. These argillaceous limestones outcrop on the Glasgow Upland, and contain poorly developed karst features (Hess *et al.*, 1989). Drainage tends to remain on the surface of these outcrops, and infiltration moves as diffuse, rather than conduit, flow. These shaley, chert-filled formations act as an aquiclude to effectively define the lower limits of the groundwater as it circulates through the entire Mammoth Cave karst aquifer (Hess and White, 1993).

Introduction to structure and stratigraphy

Deike (1967) and Hess (1976) studied the stratigraphic and structural controls on the development of Mammoth Cave and, therefore, on the permeability and major drainage lines within the aquifer. Their discussion concentrated on the controls of cavern

development and secondary permeability. Exploration and surveys have shown that Mammoth Cave consists largely of a series of low-gradient, branching conduits with higher-gradient cut-offs and vertical shafts connecting them. Cave passages follow lines of least resistance through the rock. The passages generally follow the hydraulic gradient, with a variety of relationships to dip and strike, folds, and fractures, depending on local conditions. Deike (1967) concluded that within Mammoth Cave fractures and joints exert less influence than bedding planes.

Palmer (1989) has affirmed that the variations in stratigraphy and geologic structure influence the trend and gradient of cave passages, but not the passage elevation. Most of the major passages are concordant to the local geologic structure as a result of bedding-plane partings representing the most efficient paths of flow at any given horizon within the limestone. The presence of bedding planes appears to have a greater influence on passage orientation than does the variation in lithology.

Stratigraphy and structure have influenced the regional groundwater flow pattern. The shales in the lower St. Louis and upper Salem-Warsaw Formations act as barriers to the flow of ground water and are the primary reason why the southern drainage divide is so close to the Barren River (Hess and White, 1989). The flow is generally down the structural dip in a northerly directions towards the Green River. The dip changes towards the west, at the western end of the Sinkhole Plain. The shales in that area lie below the Barren River, and groundwater flow is westward towards Graham Spring and the Barren River (Quinlan and Ray, 1989).

Stratigraphy

The overall stratigraphic sequence for the study site and surrounding area is shown in Figure 4. There are three important limestone formations and one sandstone unit associated with karst development within Mammoth Cave area. In ascending order they are the St. Louis Limestone, The Ste. Genevieve Limestone, the Girkin Limestone, and the Big Clifty Sandstone (Figure 5).

The St. Louis Limestone outcrops along the souther portion of the Sinkhole Plain. Streams that flow across the Glasgow Upland disappear at sink points in the St. Louis and become a major recharge source for the Mammoth Cave karst aquifer (Quinlan and Ray, 1989). The St. Louis consists of 40 to 80 meters of light gray to yellowish-brown, fine-to coarse-grained, thin-bedded to massive limestone with some siltstone and dolomite. The St. Louis Limestone is quite pure, with 91% to 97% calcite. Chert nodules are widespread throughout the St. Louis, but are concentrated largely in the highest and lowest zones. At the top of the formation is the Lost River Chert, which has been shown to influence both landscape and karst drainage features in the area (Howard 1968, Woodson 1981, Groves and Crawford 1990). About 12 m below the Lost River Chert is another chert bed, the Corydon Chert(Haynes, 1964). Cave streams which developed within that part of the St. Louis are often trapped under the chert, during high rain events, or flow on top of the chert bed.

The Ste. Genevieve Limestone is located above the St. Louis Limestone. It outcrops along the Sinkhole Plain closest to the Dripping Spring Escarpment and is also

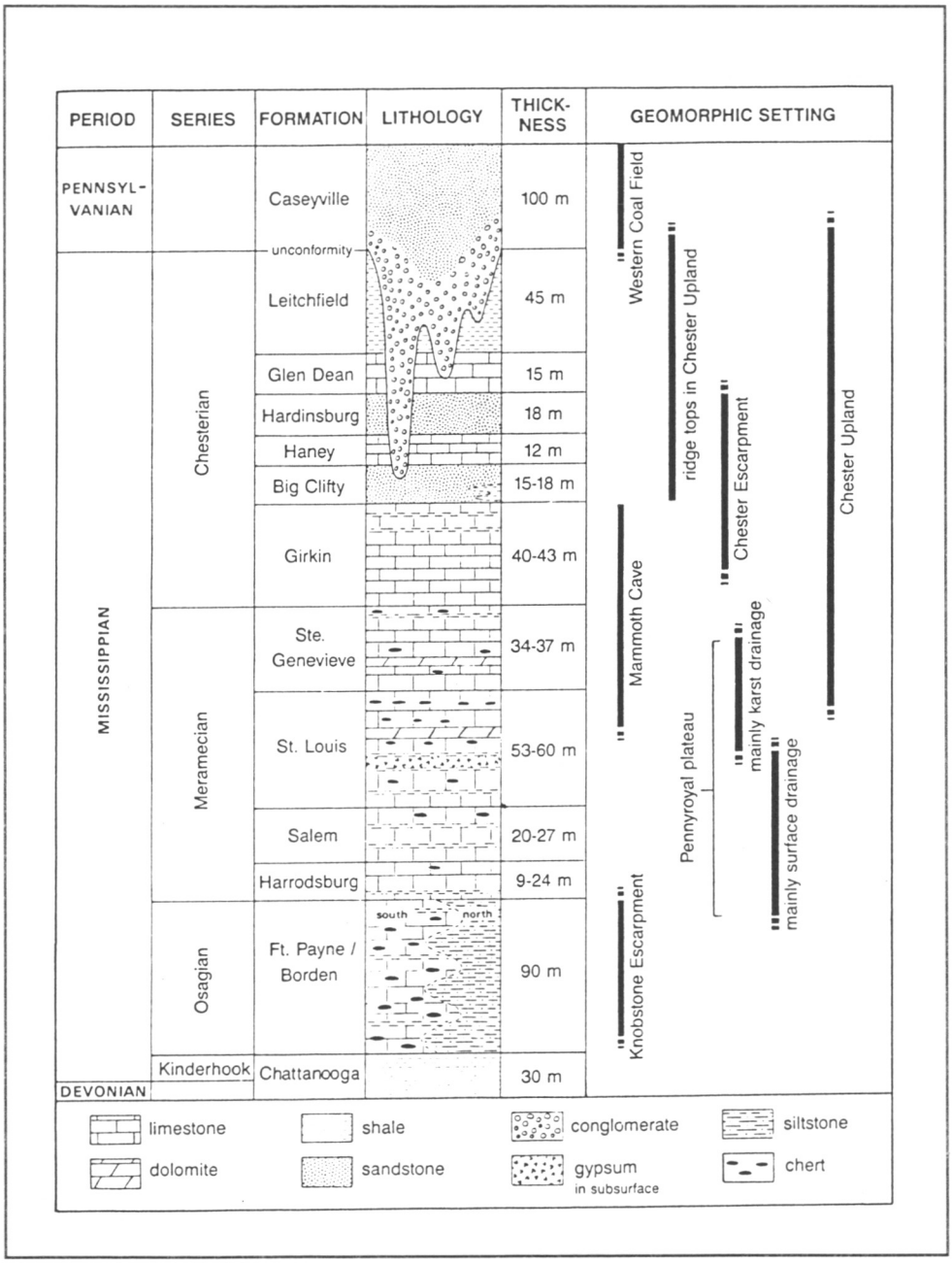

Figure 4. Stratigraphic section of the Mississippian and lower Pennsylvanian rocks of south-central Kentucky (Source: Pohl, 1970; Palmer *et al.*, 1981a).

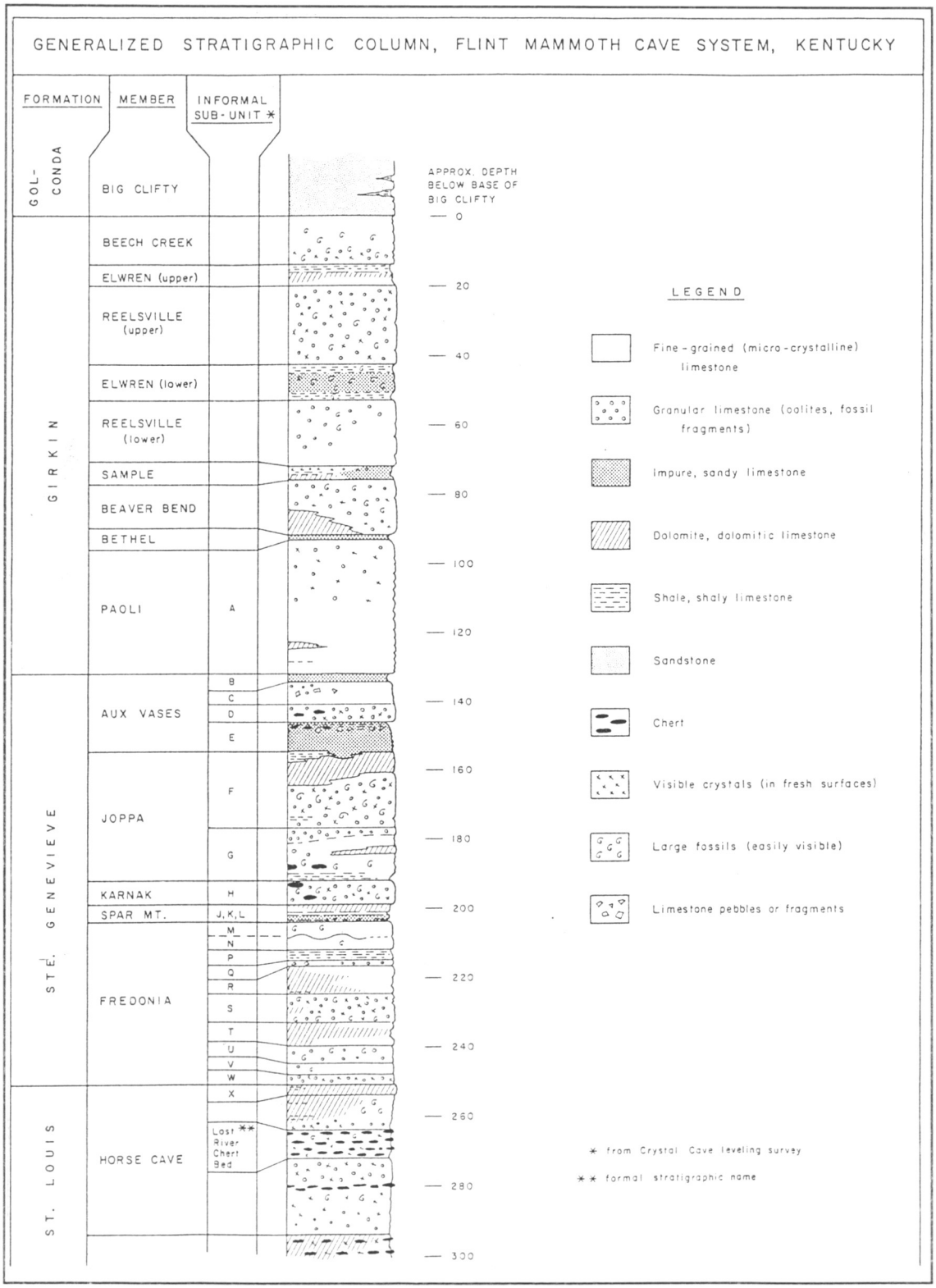

Figure 5. Generalized Stratigraphic column (Source: Palmer, 1981b).

exposed on the bottoms of the karst valleys that dissect the Mammoth Cave Plateau (Haynes, 1964). The Ste. Genevieve Limestone consists of 15 to 50 meters of white blue-gray, fine-to course-grained, locally oolitic, thin-to thick-bedded limestone. Chert zones occur in the formation but are concentrated in the lower 15 meters. Typical values of primary porosity of the Ste. Genevieve Limestone are around 3%, and the coefficient of permeability is roughly 0.002 L d^{-1} $m,^{-2}$ determined from core samples (Brown and Lambert, 1963). The Ste. Genevieve is also quite pure, commonly 95% to 97% calcite. Most of the passages within Mammoth Cave and the other related cave systems are located within the Ste. Genevieve Limestone (Palmer, 1981; Hess *et al.*, 1989). The Ste Genevieve Limestone consists of interbedded limestone and dolomite in the lower half and limestone interspersed with thin beds of competent, silty limestone in the upper half.

The Girkin Limestone is the uppermost, and Youngest, carbonate unit of the main aquifer sequence and has a considerable number of thin, interbedded shales and siltstones. The clastic units are generally less than 1 Meter thick and have only a local influence on the development of underground drainage channels (Palmer, 1981). The Girkin Limestone is considerably less pure than the St. Louis or the Ste. Genevieve Limestones, with a number of thinly interbedded siltstones and shales (Hess *et al.*, 1989). The Girkin Limestone is found under the ridges of the Mammoth Cave Plateau, but only the oldest remaining cave passages, such as Collins Avenue under Flint Ridge and the Rotunda and Gothic Avenue under Mammoth Cave Ridge, are developed in the Girkin Limestone (Palmer, 1989).

The Big Clifty, Member of the Golconda Formation, is predominately made of quartz and overlies the Girkin Limestone. An important hydrogeologic role is played by the Big Clifty Member; it acts as a protective caprock that retards the erosion and dissection of the Mammoth Cave Plateau and is responsible for the steep south- and east-facing escarpment that marks the edges of the plateau (Hess *et al.*, 1989). At the base of the Big Clifty are a few meters of discontinuous black shale. Where the shale is present, vertical percolation of groundwater is essentially nonexistent. Where the shale is absent, some percolation apparently occurs although most of the vertical infiltration is at the margin of the caprock at Mammoth Cave Plateau's edge (Hess *et al.*, 1989). Near the top of the Big Clifty is an organic-rich zone containing quantities of pyrite, which might be the source of sulfate minerals found in the cave systems (Hess *et al.*, 1989).

Above the Big Clifty Member is a shallow, 12 meters thick limestone unit called the Haney Limestone Member of the Golconda Formation (Haynes, 1964). The Haney is a well-jointed crystalline limestone which forms a minor aquifer, perched well above the Mammoth Cave karst aquifer (Hess *et al.*, 1989). This unit outcrops on Flint Ridge south of the Green River and in the dissected Hilly Country north of the Green River (Hess *et al.*, 1989). At Flint Ridge, the Haney Limestone provided small springs used by the early settlers of the area (Cushman *et al.*, 1965). The Haney springs, vertical shafts, and karst valleys contribute to both local and regional springs that drain the Mammoth Cave Plateau (Hess *et al.*, 1989).

Structure

On a regional scale, the south-central Kentucky karst is developed within a structural monocline with rocks dipping gently to the northwest. To the east, the Cincinnati Arch is a broad anticlinal flexure that extends from the Lexington Dome in the north to the Nashville Dome in the south. Toward the northwest is the Illinois Basin. North of the Mammoth Cave area, an outcrop line of Mississippian rocks extends parallel to the Cincinnati Arch continuously into southern Indiana. West of the Mammoth Cave area, the outcrop line of Mississippian rock parallels the Illinois basin westward to the Mississippi River Embayment.

On a local scale there is much fine detail to the structure. The structural contour map (Figure 6) shows the general northwest-trending dip broken by minor flexures with axes oriented perpendicular to the regional strike and many minor structural highs and structural troughs (Hess *et al.*, 1989). A sudden steepening of the dip does occur in an east-west pattern and has considerable influence on the geometry of the Dripping Spring Escarpment as well as groundwater flow (Howard, 1968).

Faulting is most pronounced in the northern part of the region where normal faults with throws of tens of meters have been found. There are also many smaller faults, mostly unmapped, with throws of a few meters or less scattered throughout the region. On the south side of the Green River their influence on the structure is generally negligible (Hess *et al.*, 1989).

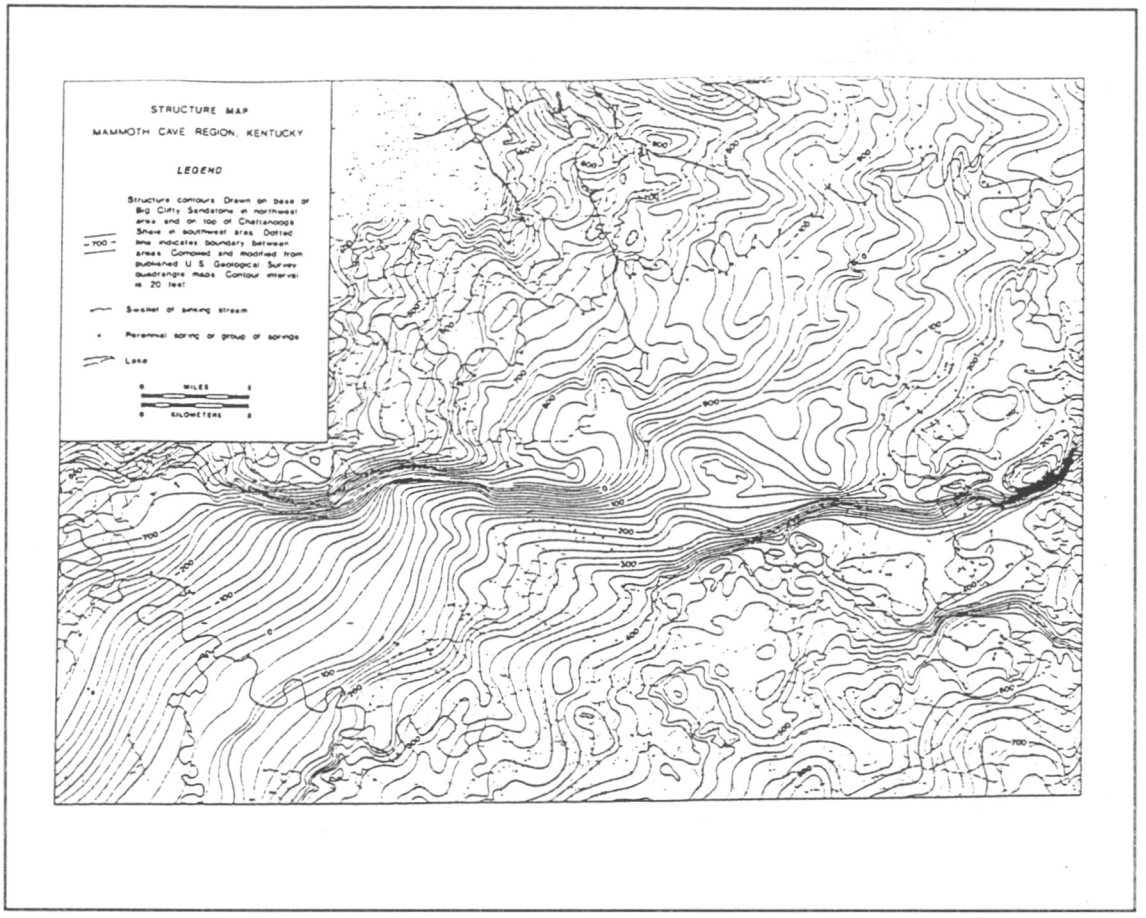

Figure 6. Geologic structure of the Mammoth Cave area (Source: Quinlan and Ewers, 1981).

Surface hydrology

The Mammoth Cave karst area lies entirely within the drainage basin of the Green River, (Figure 7), which flows in a meandering channel from east to west as shown in the upper portion of the map. The Green River has two main tributaries in the area, the Barren and Nolin Rivers. The Barren River flows from the south and east and drains much of the southern portion of the Green River Valley. The Nolin River flows from the northeast and enters the Green River as depicted in the north-central portion of the map.

The Nolin River flows mainly over the thick clastic rocks that lie above the cave-forming limestone.

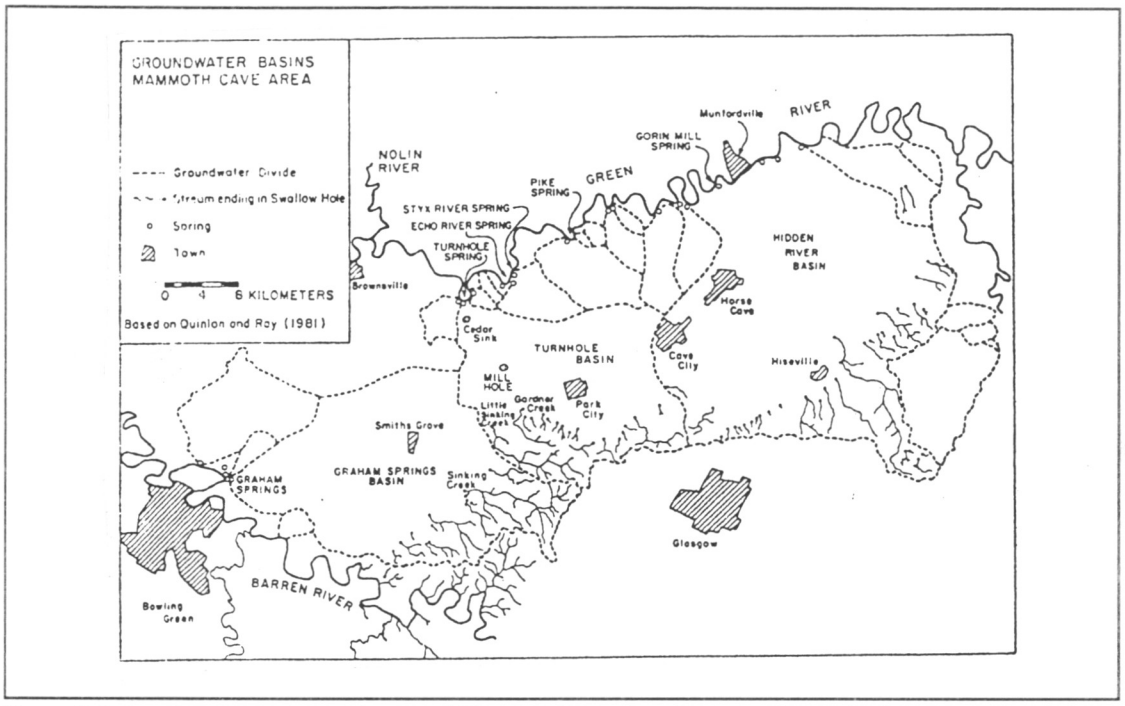

Figure 7. Map of a portion the south-central Kentucky karst showing groundwater basins (Source: Quinlan and Ewers, 1989).

The first-order drainage basin of the south-central Kentucky karst is defined by a series of smaller drainage divides. There is a distinct drainage divide along the southern margin of the Sinkhole Plain. To the south there are surface tributaries to Beaver Creek and Little Barren River on the Salem, Harrodsburg Warsaw, and Fort Payne Formations (Hess *et al.*, 1989). North of this divide there is surface drainage consisting of short segments of streams that flow northward toward the Sinkhole Plain. The water then generally sinks in the middle of St. Louis Limestone upon reaching the purer limestones of the formations upper half. The drainage divide is south of the physiographic boundary

between the Sinkhole Plain and the Glasgow Upland. An eastern boundary is the Little Barren River, which drains north into the Green River from the Glasgow Upland. An equivalent western boundary would be the Barren River (Hess *et al.*, 1989).

Subsurface hydrogeology

The major hydrologic base level for the Mammoth Cave region is the meandering Green River. The Green River is generally 15-30 m wide and usually less than 8 m deep; it also extends some 64 km and receives discharge from some 81 springs in the area (Hess *et al.*, 1989). There are several sources that supply the water discharging from base-level springs. These sources include precipitation that recharges perched aquifers, sinking streams, sinkhole areas, and back-flooding water from the Green River into base-level aquifers. The Sinkhole Plain catchment makes up 47% of the total area and 60% of the area south of the Green River. The Chester Cuesta catchments make up 53% of the total area, 100% of the area north of the river, and 40% of the area south of the river (Hess *et al.*, 1989)

A conceptual model for the groundwater system and overall hydrologic arrangement for the south-central Kentucky karst is illustrated in Figure 8. The model shows that south-central Kentucky karst aquifers have both diffuse-flow and conduit-flow components. Diffuse-flow aquifers are those in which groundwater movement takes place on (or mainly) through the primary permeability and the fracture permeability. Conduit-flow aquifers are those that have a well-developed conduit permeability (Shuster

and White, 1971).

The main groundwater body in the south-central Kentucky karst area occurs in the cavernous St. Louis, Ste. Genevieve, and Girkin Limestones. Cavernous limestone is often described in terms of the overall permeability of the carbonate rock. The permeability can be characterized by the sum of three contributions (White 1988):

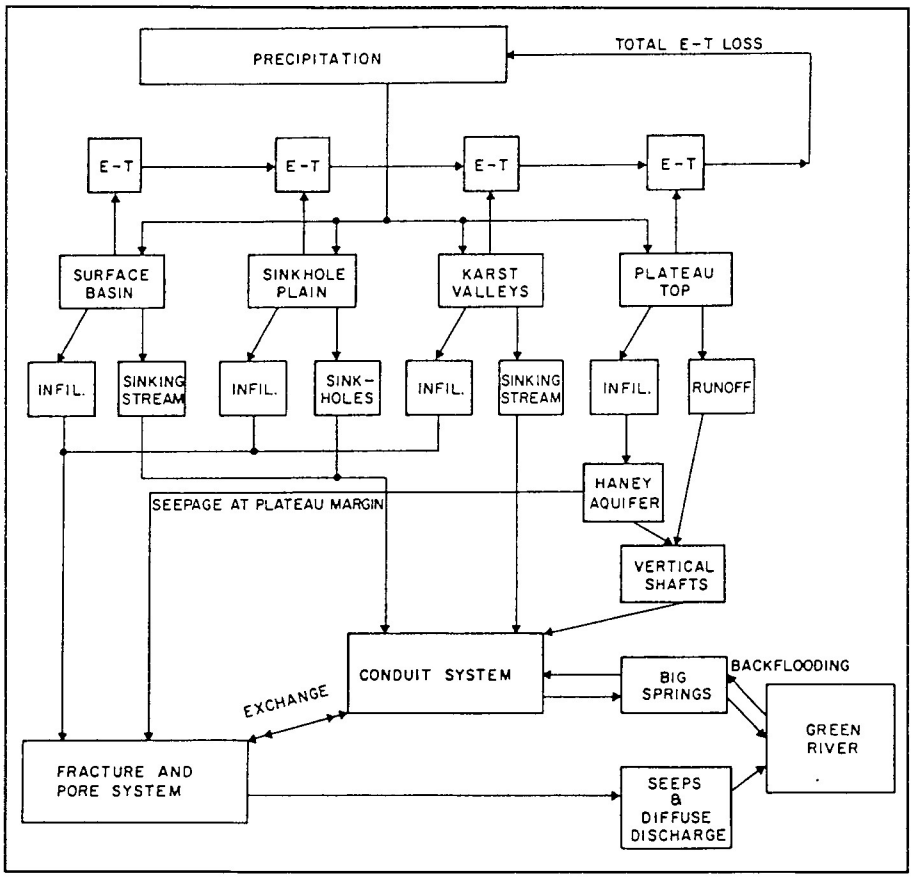

Figure 8. Conceptual model for groundwater and surface-water flow systems in the south-central Kentucky karst (Source: Hess *et al.*, 1989).

1. Primary porosity and permeability that is due to the presence of communicating pore

spaces;

2. Permeability that is due to the three-dimensional network of joints, fracture, and bedding-plane partings;

3. Permeability due to cavernous openings.

The primary porosity of the Ste. Genevieve Limestone, for example, is around 3 % and the coefficient of the permeability is roughly 0.002 L d^{-1} m^{-2}, as determined from core samples (Brown and Lambert, 1963). Specific capacities of wells drilled in the St. Louis Limestone range from 70 to 8,700 L min^{-1} m^{-1} of drawdown.

Sediments

Vast amounts of clastic sediment have been deposited within most of the passages within the Mammoth Cave System. It is not unusual to find passages that have been filled nearly to their ceilings (Figure 9). In some areas the nature of the stratigraphic sequence has only been revealed in areas where the sediment has been washed away by more recent cave streams, or dug out for public trails. Water flowing through the Mammoth Cave System has been the primary means of transport for large quantities of clastic sediment. Subsurface water moving through Mammoth Cave transports sediment as dissolved load, suspended load, and bedload (White and White, 1968). There are various possible sources for the sediment within an open flow conduit: (1) sediment transported from a distant source by a sinking surface stream; (2) surface soil infiltrating through sinkholes; (3) debris from overlying clastic rocks falling directly into the channel

through vertical shafts; (4) insoluble detritus from the limestone transported from one location to another; (5) sediment from base-level back-flooding of a nearby river carried into the conduit against the normal gradient (White and White 1968).

The clastic sediments within Mammoth Cave have been generally described as either internally derived autochthonous deposits (breakdown [limestone blocks

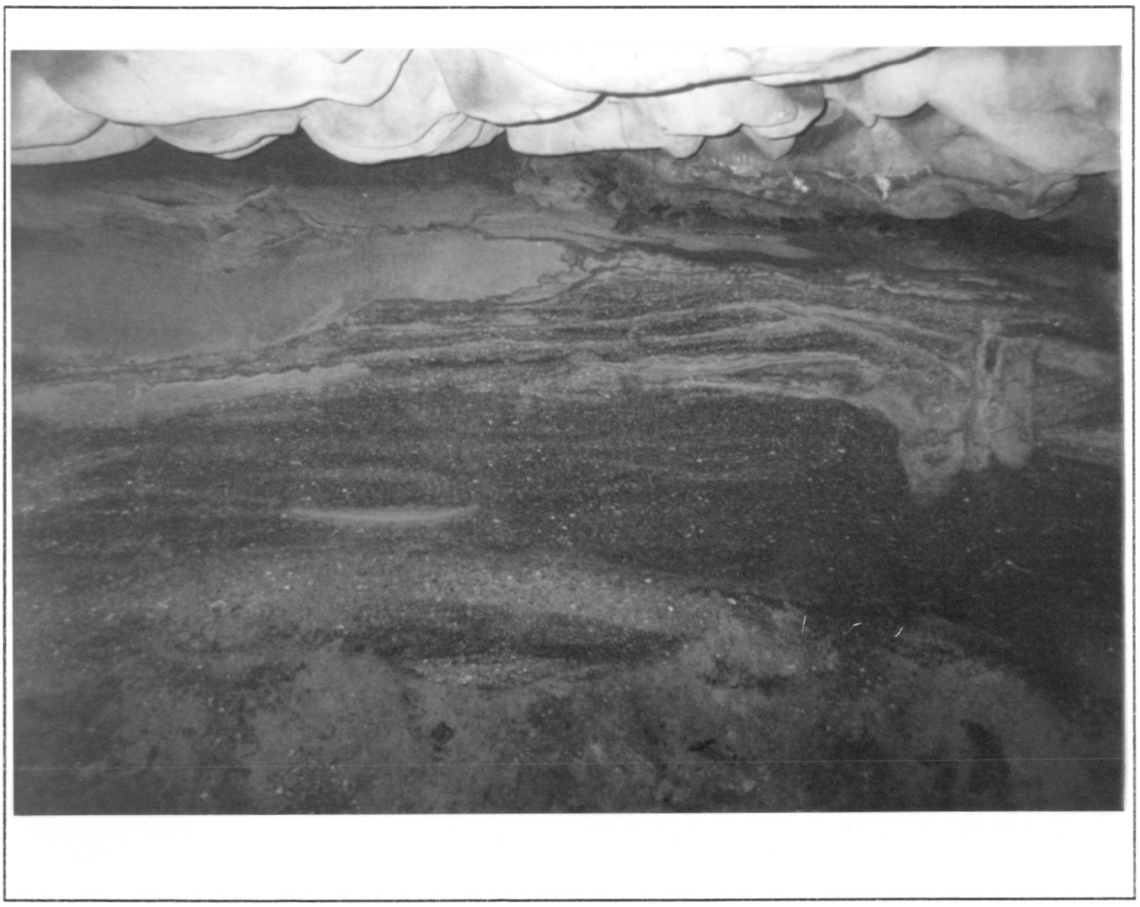

Figure 9. Stratified layers of clastic sediment that filled to the ceiling in the Old Women's Bathroom at Mammoth Cave, Kentucky.

that fall from either the ceiling or the walls], weathering detritus, and organic matter) or as externally delivered allocthonous deposits (transported clay, silt, sand, gravel, and

loess) (White and White 1968). The clastic sediment resulting from breakdown is generally limestone and is readily dissolved and removed in solution. The insoluble residue of clay, silt, sand, fossil fragments and chert that are left behind after the limestone dissolves is known as weathering detritus. The amount of insoluble residue depends on the purity of the original limestone. Organic matter has been transported into some areas of Mammoth Cave as either a result of back flooding from the Green River, sinking streams, or through vertical shafts (White and White, 1968).

An extensive classification of the stratified layers of sediment exposed by excavated trails throughout many different passages was performed by Davies and Chao (1959). Most sediments were red-brown, brown, or gray in color. Davies and Chao (1959) found that silt is the most extensive type of fill in Mammoth Cave. In addition to the silt, most sediments contain 5% to 20% percent fine sand and about the same amount of clay. In general, the red-brown sediments have a higher clay content than those that are brown or gray.

Fine sand and mixtures of silt and sand were found to be very common in many of the fills in Mammoth Cave. Sand fills showed little variation in distribution of grain size and generally were white, tan or reddish brown. Pure clays are rare in Mammoth Cave (Davies and Chao, 1959), but a smaller amount of clay can be found intermixed within the sand and silt. Mixtures of silt and clay, most frequently present near the tops of many fills as the last phase of deposition, are commonly red to red-brown in color and are generally laminated.

It has been theorized that the layers of stratified sediments within many cave passages play an important role in the dissolution of the limestones. Sediment beds, for example, may insulate the soluble limestone floor from the solutional attack of moving water. Therefore, if the velocity of the subsurface stream is sufficient to move the bed load, but not fast enough to lift it into suspension, the limestone floor may not be exposed to solutional or abrasive attack from the circulating groundwater.

According to White and White (1968) sediment beds can act as a self-perching mechanism which forces the cave stream to flow at its original level, preventing the river from down cutting its channel. Then as base level is lowered, an increased local hydrostatic head is generated within the aquifer due to the perched stream. Eventually this head will provide the driving force for cutting a new solution channel on a lower level. The original channel may then be abandoned or carry only a fraction of its former flow, thereby providing an additional mechanism for the formation of two distinct passages separated vertically from each other rather than one deep canyon.

Logsdon River studies

The Logsdon River conduit in the Mammoth Cave System is the primary drain for the Cave City, Kentucky, groundwater sub-basin. It is also the longest accessible river conduit in the entire Mammoth Cave karst aquifer (Anthony, 1998). In the mid-1990's the National Park Service began continuous monitoring of the Logsdon and Hawkins River for the primary purpose of understanding the effects of storm and seasonal changes

on the water quality of these two streams. Continuous monitoring at the Logsdon River well produced some remarkable results: (1) A strong statistical relationship between conductivity and the dissolved constituents calcium, magnesium, and bicarbonate were found to exist (Groves and Meiman, 1995a, and 1996) and (2) at least part of the year, during low-flow conditions, the water flowing past the Logsdon River well was oversaturated with respect to calcite (Groves and Meiman, 1996). These oversaturated conditions were not expected since earlier studies on sinking steams on the Sinkhole Plain and regional springs on the Green River had found these waters are generally undersaturated with respect to calcite (Hess, 1974; Hess and White, 1989). A convincing explanation for changes in the geochemistry at the Logsdon River conduit has been proposed by Anthony (1998), who found that the Logsdon River moved from supersaturated to undersaturated conditions as a result of an in-cave source of CO_2,- namely, the microbial decomposition of organic materials.

Since a large subsurface river, such as the Hawkins River, is able to change from oversaturated to undersaturated conditions as a result of microbial decomposition of organic matter, these processes may also impact the interstitial fluid. It therefore may be possible that decomposition of organic matter within the clastic sediment beneath the aquifer stream may cause the interstitial fluid to be more undersaturated with respect to calcite than the active stream.

The study site

Mammoth Cave has extensive conduits covering more than 560 kilometers, with five different levels that extend through three different limestone units. This study was conducted within the active stream systems of River Styx and Echo River, beneath Mammoth Cave Ridge. The majority of the research on the interstitial fluid behavior in a cave aquifer conduit took place at the upper end of the distributary of the River Styx, near the base of Charon's Cascade (Figure 10). Charon' s Cascade is a waterfall that flows from the ceiling roughly 8 meters above the floor at a rate of approximately 0.5 to 3 L s^{-1} During base flow conditions Charon's Cascade falls directly onto the sediment, travels a short distance and flows into the River Styx. After a significant rain event, when the Green River and the River Styx is about three or more meters above base flow, Charon's Cascade will fall directly into the River Styx.

Echo River and the River Styx are the main underground drainage areas for Mammoth Cave Ridge and adjacent karst valleys (Palmer, 1981). The River Styx receives most of its flow from the organic-poor soils of the Mammoth Cave Plateau and experiences a very small seasonal change in CO_2 partial pressure (Miotke 1975, Hess *et al.*, 1989, and Hess and White 1993). The River Styx primarily acts as a subsurface overflow route for Echo River, and the water eventually discharges as a spring along the Green River. At the location of the study site at the upper end of the River Styx water flows through the upper levels of the St. Louis Limestone. Access to the River Styx site

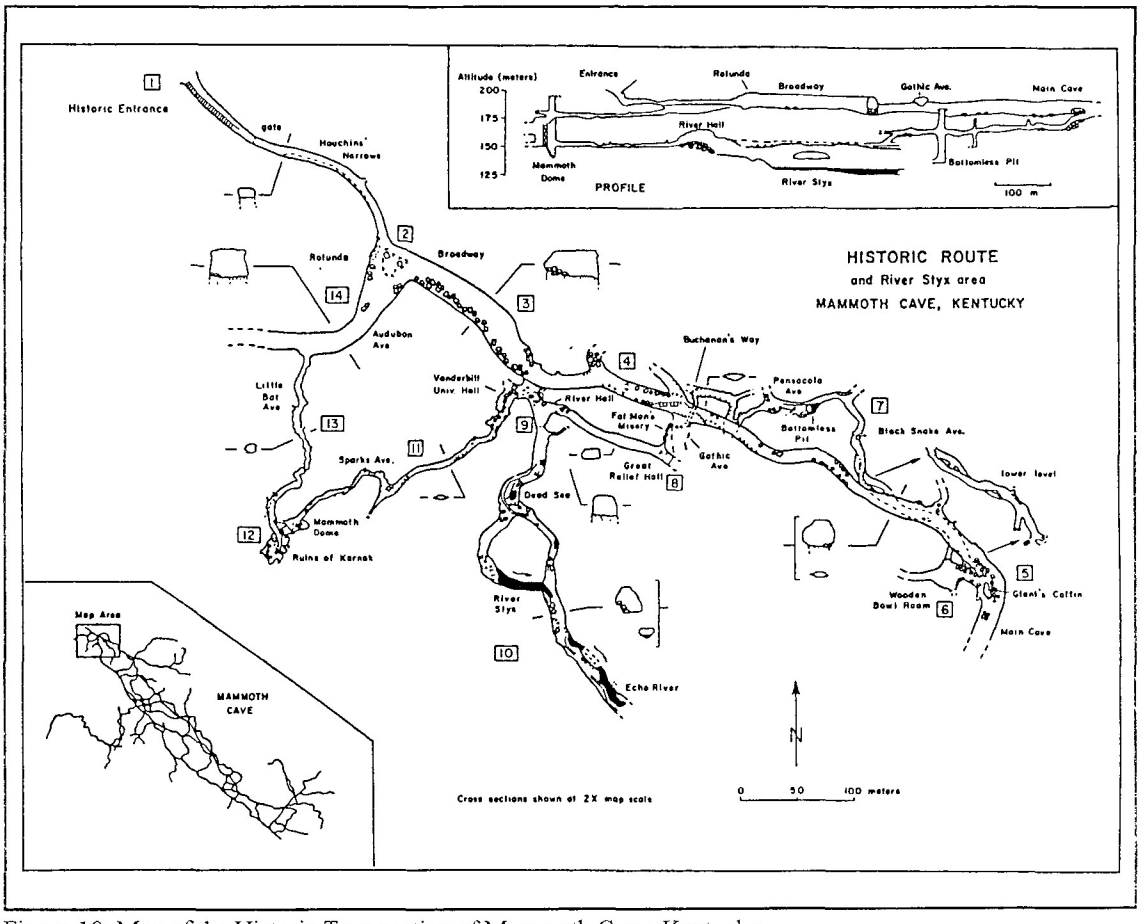

Figure 10. Map of the Historic Tour section of Mammoth Cave, Kentucky.
Source: Palmer, 1981.

can be gained through the Historic Entrance of Mammoth Cave and the old tourist path that leads to the river.

Echo River receives most of its flow from the organic-poor soils of the Mammoth Cave Plateau and consequently demonstrates a very small change in CO_2 partial pressure (Miotke 1975, Hess *et al.*,1989, Hess and White 1993). Echo River has been a major river system, but under current flow conditions the headwaters have been pirated by Turnhole Spring (Quinlan and Rowe, 1978) and the original route to Echo River

concurrently acts as an overflow basin to Turnhole Spring (Quinlan and Ray, 1989, and Meiman and Ryan, 1993). The River Styx has a complex hydrogeology. During base flow, when the volume of sediments that are in transport are minimal due to low velocity conditions, the River Styx receives local shaft inputs from the edge of the Mammoth Cave Ridge, and epikarst waters follow a portion of Houchin's Valley. During high flow conditions, when the Logsdon River stage is three or more meters above base, the River Styx receives overflow water from Cave City Patoka Creek and Proctor Subbasins (sinkhole Plain, and sinking creeks). During flow reversal of the River Styx Spring, usually when the River Styx is about 2 meters above base with no local precipitation, the River Styx receives an influx of water, sediment, organic material from the Green River (Meiman and Ryan, 1993).

CHAPTER III

CARBONATE CHEMISTRY BACKGROUND

Introduction

The purpose of this study is to measure and understand water-rock interactions at the water-rock interface beneath the clastic sediment of a major base level conduit within the Mammoth Cave System and to determine what effect the clastic sediment has on limestone dissolution at the contact between the sediment and the underlying bedrock.

Within the south-central Kentucky karst, caves have been formed by the dissolution of bedrock by circulating groundwater. Although much effort has been expended on determining limestone dissolution rates they have not been measured within and beneath the clastic sediment of active cave passages. This research effort was an attempt to understand the geochemical environment of the interstitial fluids within the sediment beneath an active flowing stream channel. The collected data were used to test how limestone dissolution rates occur at the water/rock interface beneath the sediment and within the overlying clastic sediment. Water samples were collected and analyzed at various levels throughout the deposited sediment.

Study of the details of limestone dissolution is crucial for understanding the developmental processes within karst landscapes. Rates and mechanisms of limestone dissolution in carbonic acid solutions have been widely studied, and several theoretically and empirically derived dissolution models, or rate expressions, have been developed to

predict dissolution rates as a function of water chemistry and flow conditions (Curl, 1965; Berner and Morse, 1974; Plummer and Wigley, 1976; Plummer *et al.*, 1978 and 1979; Dreybrodt, 1981; Palmer, 1991). For example, their dissolution models have shown that if the mineral calcite is in contact with highly acidic dissolving fluids the rate of calcite dissolution will also depend on the rate of discharge of the fluids. These expressions also provide information on the small-scale details of the dissolution process and are central elements of theoretical models of karst aquifer and landscape development (Dreybrodt, 1988 and 1990; Palmer, 1981, 1984, and 1991; Groves and Howard, 1994a and 1994b; Howard and Groves, 1995) enabling us to study aspects of karst evolution which occur at temporal and spatial scales that prevent direct observation.

Carbonate analysis

Measuring the constituents within the sediment was very important in understanding the nature of the processes that occur with respect to limestone dissolution. Within carbonate areas calcium forms the dominant cation within groundwater (Langmuir, 1971). Natural water is very rarely pure and generally contains varying amounts of minerals, salts, pollutants, and metals and is seldom found to have a neutral pH of 7 (Drever, 1997). Unpolluted rain water in equilibrium with the atmosphere ($Pco_2 = 10^{-3.5}$ atm) at 25° C generally has a pH of 5.6, and has the ability to dissolve limestone. In reality, the pH of rain is quite variable, influenced by other solutes (particularly acids) derived from the atmosphere (Drever, 1997); typical pH range of

Mammoth Cave area rain water is 3.5 to 5.0.

The limestones within the Mammoth Cave area are quite pure, roughly 97% pure, and are predominantly made of calcite and a smaller amount of impurities (Palmer, 1981b). Calcite ($CaCO_3$) is an ionic salt, and in natural water it will dissociate into its constituent ions as follows:

$$CaCO_3 \Leftrightarrow Ca^{2+} + CO_3^{2-}. \quad (1)$$

The dissolution of $CaCO_3$ in natural waters is generally a reaction with the combination of carbon dioxide and water:

$$CaCO_3 + CO_2 + H_2O \Leftrightarrow Ca^{2+} + 2\,HCO_3. \quad (2)$$

The dissolution of calcite has been shown to occur by three simultaneous forward reactions (Plummer *et al.*, 1978):

$$CaCO_3 + H^+ \Leftrightarrow Ca^{2+} + HCO_3^-, \quad (3)$$

$$CaCO_3 + H_2CO_3 \Leftrightarrow Ca^{2+} + 2\,HCO_3, \quad (4)$$

$$CaCO_3 + H_2O \Leftrightarrow Ca^{2+} + HCO_3^- + OH^-. \quad (5)$$

Once activities of each of the appropriate species have been determined for a particular solution, the equilibrium state of the solution can be obtained by writing a mass action expression for the reactions of interest. For example, for the following reaction

$$aA + bB \leftrightarrow cC + dD; \quad K_{eq}\ , \tag{6}$$

equilibrium activities are given by

$$K_{eq} = \frac{[C]^c[D]^d}{[A]^a[B]^b} \tag{7}$$

where brackets denote activities and k_{eq} is a temperature dependent equilibrium constant for the reaction.

The carbonate ions that form by the dissociation of alkaline earth carbonates hydrate when in contact with water (White, 1988)

$$CO_3^{2-} + H_2O \leftrightarrow HCO_3^- + OH^- \tag{8}$$

forming a mildly alkaline solution. Increasing the hydroxyl concentration by raising the pH decreases the carbonate solubility. However, introducing hydrogen ions by lowering the pH drives the reaction to the right, greatly increasing carbonate solubility (White, 1988). Most carbonate minerals are readily soluble in acid and the acid most important

to karst processes is carbonic acid, formed by the dissolution of gaseous CO_2 and water H_20.

The solution of carbon dioxide from the gas phase takes place in two steps. First CO_2 gas is transported across the gas-liquid interface to form CO_2 (aqueous) in solution. The dissolved CO_2 then reacts with water to form carbonic acid. There is no simple way to distinguish the two reactions, and they are usually considered simultaneously (White, 1988).

$$CO_{2_{(gas)}} \Leftrightarrow CO_{2_{(aq)}} \tag{9}$$

$$CO_{2_{(aq)}} + H_2O \Leftrightarrow H_2CO_3 \ . \tag{10}$$

For reaction (10) a mass action expression can be written

$$K_{CO_2} = \frac{aH_2CO_3}{P_{CO_2}}, \tag{11}$$

where Pco_2 is the carbon dioxide partial pressure expressed in atmospheres. The concentration of dissolved CO_2 increases with increasing carbon dioxide pressure in the gas phase that coexists with the aqueous solution. Dissolved CO_2, however, decreases with increasing temperature (White, 1988).

Carbonic acid dissociates in solution to form the bicarbonate ion

$$H_2CO_3 \Leftrightarrow H^+ + HCO_3^-, \quad (12)$$

which in turn dissociates to form the carbonate ion

$$HCO_3 \Leftrightarrow H^+ + CO_3^{2-}. \quad (13)$$

At the pH and ionic strength of most karst waters, the bicarbonate ion is the dominant inorganic carbonate species (Figure 11).

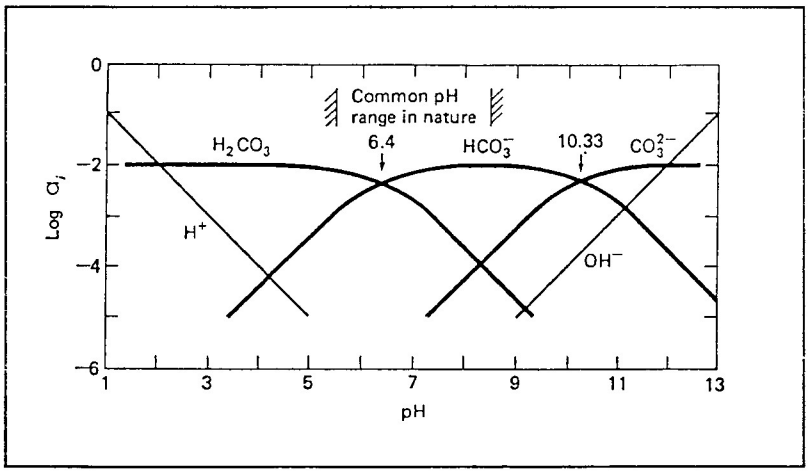

Figure 11. Activities of different species in the carbonate system as a function of pH, assuming $\sum CO_2 = 10^{-2}$, temperature = 25°C. Activities of H^+ and OH^- are defined by pH (Source: Drever, 1997).

The activity of the carbonate ion links these reactions to the solubility of calcite and dolomite. The activities of calcium and magnesium are determined directly from the

measured concentrations. The activity of CO_3^{2-} is a minor species at the pH of most karst waters, and is calculated from the pH and bicarbonate (Drever, 1997)

$$aCO_3^{2-} = \frac{aHCO_3 \; K_2}{aH^+}, \qquad (14)$$

where K_2 is the equilibrium constant for reaction (13).

The activity of H^+ may be controlled by other reactions in the system (White, 1988). When CO_2 gas is brought into contact with water, the CO_2 will dissolve until equilibrium is reached. At equilibrium, the concentration of dissolved carbon dioxide will be proportional to the pressure (fugacity) of CO_2 in the gas phase. At earth-surface conditions, the difference between partial pressure and fugacity can be ignored (Drever, 1997). It is common practice to refer to all dissolved carbon dioxide as H_2CO_3 (carbonic acid). Carbonic acid is a weak acid, but it has the ability to dissolve limestone.

The dissolution of limestone (eqn. 2) will not take place if the water in contact with the rock is at equilibrium. Due to the typical short residence times for water within karst aquifers compared to the longer time scale of dissolution kinetics, karst waters are rarely in equilibrium with solid calcite (Wollast, 1990). Many karst waters are undersaturated with respect to calcite and are thus capable of dissolving limestone. Supersaturated karst water may precipitate calcite as features known as speleothems or travertine through a process of nucleation and precipitation (White, 1988). A convenient

way of expressing whether a solution is supersaturated or undersaturated to a particular solid phase is by describing the solution in terms of a saturation index.

A saturation index value for a particular water/rock interaction can be expressed as

$$SI = \log_{10} \left(\frac{IAP}{K_{eq}}\right) \tag{15}$$

where

SI is the saturation index,

IAP is the ion activity product for the reaction of interest, and

K_{eq} is a temperature dependent equilibrium constant for the reaction of interest.

The activities are related to concentration by the equation

$$a_i = \gamma_i \, m_i \tag{16}$$

where

m_i is the molal concentration for species *I*, and

γ_i is the activity coefficient.

The activity coefficient, γ_i, relates the activity, a thermodynamically idealized concentration, to the measured concentration. In an ideal infinitely dilute solution the activity coefficient is equal to one ($\gamma_i = 1$). Activity coefficients can be calculated for

each ion in dilute solutions by means of the Debye-Hückel equation (Stumm and Morgan, 1981)

$$\log \gamma_i = \frac{Az_i^2\sqrt{I}}{1 + Ba_0\sqrt{I}} \quad (17)$$

where

z is the charge of the ion *I*,

A is a constant depending on temperature,

I is the ionic strength of the solution,

B is a constant depending on temperature, and

a_0 is the hydrated radius of the particular ion.

Ionic strength, I, is a measure of the total concentration of charged species in solution, and can be defined as follows:

$$I = \frac{1}{2}\sum m_i z_i^2 \quad . \quad (18)$$

The predicted direction of water/rock interactions can be determined for the interstitial fluids within clastic sediments by calculating the fluid's saturation index with respect to a given ion. For example, a positive saturation index will predict that calcite

precipitation may occur. A zero saturation index value indicates the water is at equilibrium with respect to calcite. A negative saturation index value predicts that the water is undersaturated and would thus dissolve calcite.

The saturation index for calcite is given by

$$SI_{cal} = \log \left(\frac{aCa^{2+} \quad aCO_3^{2-}}{K_{cal}}\right) \tag{19}$$

where

K_{cal} is the equilibrium constant for the calcite dissolution reaction.

Dissolution kinetics

The carbonate mineral, calcite, is among the most reactive minerals found at the Earth's surface (Wollast, 1990). The dissolution and precipitation of calcite from aqueous solutions plays a major part in various geological environments, especially in the formation of karst landscapes (Dreybrodt, 1987, 1988, 1989, 1990, 1992), early diagenesis in marine sediments (Sjöberg, 1978, Berner 1980, Murray *et al.*, 1980, Keir, 1982, Morse, 1983, Sayles, 1985, and Boudreau, 1987), or the evolution of downstream water chemistry in rivers (Suarez, 1983, Herman and Lorah, 1987, and Dreybrodt, 1992).

Since most natural waters are rarely in equilibrium with respect to calcite (Drever, 1997) a reaction towards equilibrium will occur. Usually, one step in the dissolution process is much slower than all the others, and the rate of this step, the rate-determining

step, determines the rate of the overall dissolutional process. There are two fundamental types of rate limiting steps: transport and reaction limited. Transport refers to the physical movement of chemical species to and from the site of reaction. Reaction limited refers to the rate of formation or destruction of chemical bonds (Drever, 1997).

Transport-limited dissolution occurs when either the flow velocities of the solution are very slow or when the solution has very high degrees of undersaturation. Based on the Reynolds number and the flow velocities of the clastic sediment a theoretical dissolution rate equation, for the limestone within the sediment, was developed with the assumption that it was a transport limited process (Berner and Morse, 1974).

Reaction-limited dissolution occurs when either the detachment from the solid phase is slow or when the flow conditions are turbulent. The surface stream at the base of Charon's Cascade can be considered as turbulent flow conditions. The well-known rate expression of Plummer *et al.* (1978) was used to predict the amount of dissolution that would occur based on the assumption that dissolution was a reaction limited processes.

CHAPTER IV

METHODOLOGY

Introduction

The River Styx/Charon' s Cascade area within the Mammoth Cave System was chosen as the site for an in-depth study of the baseflow geochemistry of interstitial fluids for several reasons. First, Charon' s Cascade conduit has a continuous flow of water (Figure 12). Second, the path leading from the entrance to the river is paved and easily accessible. Third, the National Park Service and the Center for Cave and Karst studies at Western Kentucky University, under the direction of Mr. Joe Meiman and Dr. Chris Groves, are current sponsors of a joint long-term study of the hydrology and geochemistry of the Mammoth Cave Karst Aquifer.

Four methods were used to study flow and water/rock interactions beneath the sediment of the Mammoth Cave karst aquifer at Charon's Cascade. These methods include collection of water samples, a limestone weight loss experiment, sediment profiling, and simple numerical modeling of the interstitial fluid flow based on field data.

Chemical measurements

A. Water sampling. Data for this project were primarily collected from

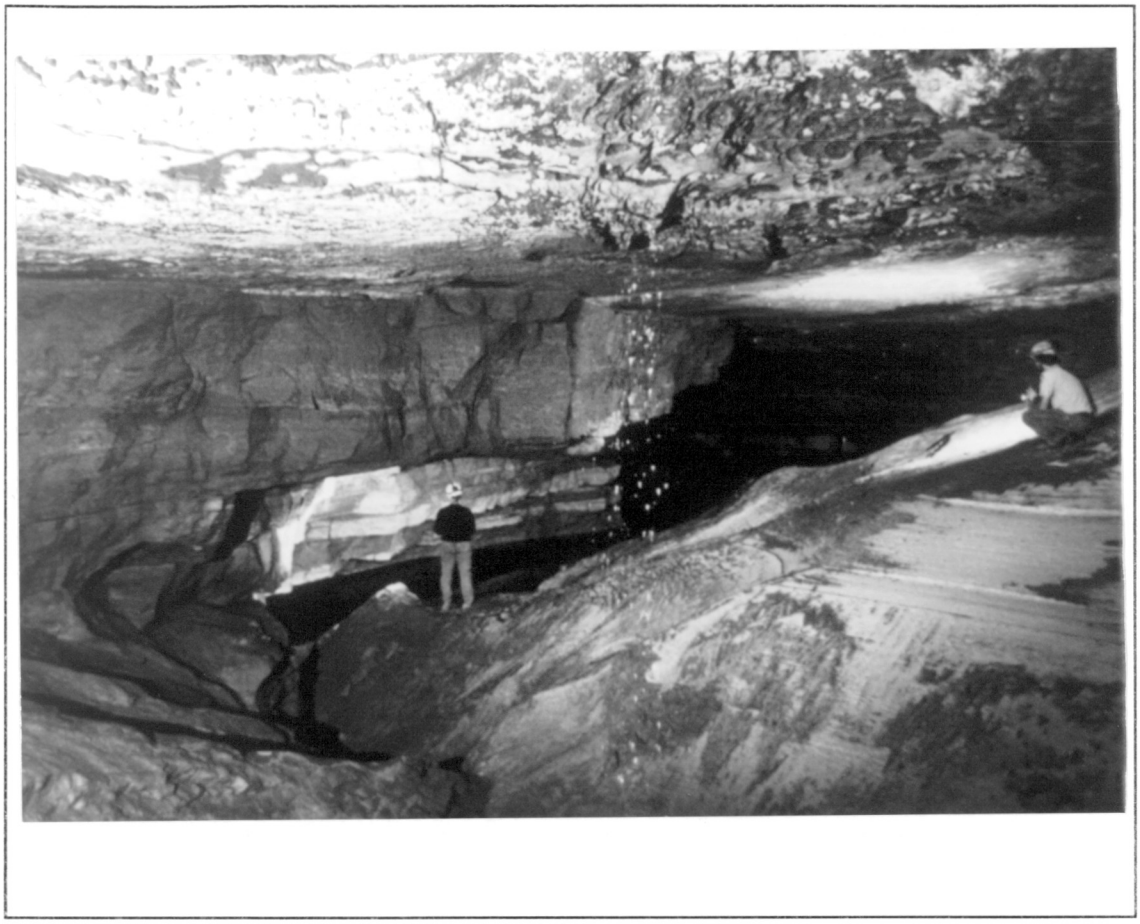

Figure 12. Charon's Cascade and the River Styx at Mammoth Cave, Kentucky.

onsite field sampling. Temperature, pH, calcium, bicarbonate, and magnesium were measured from water samples taken from within the sediment at various depths: 90 cm, 60 cm, 30 cm, and 15 cm below the open stream and within the stream (Figure 13). The water samples were collected from a nest of small diameter piezometers at the field site (Figure 14). These samples were then poured into sealable water containers that were

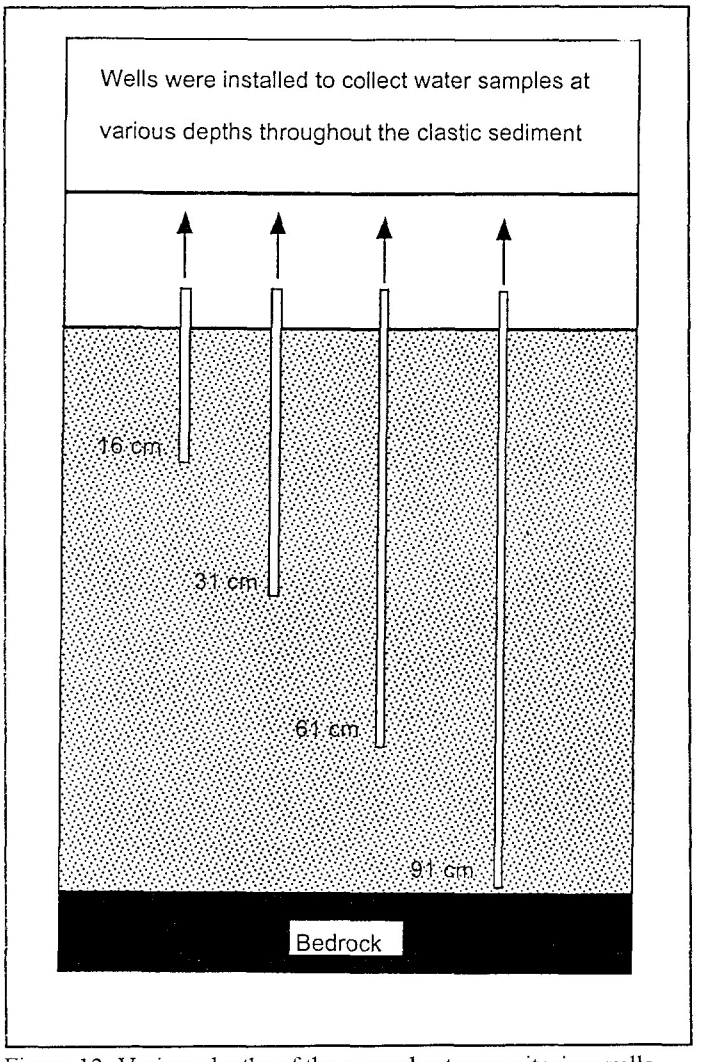

Figure 13. Various depths of the groundwater monitoring wells placed within the sediment at the base of Charon's Cascade at Mammoth Cave, Kentucky.

kept on ice at 4^0 C, the temperature at which water attains it maximum density. As soon as a water sample was collected, the pH, temperature, and conductivity were measured. The pH was measured through the use of a Cole Parmer pH meter with a two-point calibration that reports to the nearest 0.02 pH units.

The water samples were then transported to Mammoth Cave National Park's water lab for further analysis. The water samples were then filtered with a .45 μm

Figure 14. Groundwater monitoring wells and the angle braces with the limestone tablets at the base of Charon's Cascade at Mammoth Cave, Kentucky.

membrane filter. After filtering, the water samples were then measured for calcium and alkalinity concentrations by titration methods based on Standard Methods 3500 - Ca D (Greenberg et al., 1992) and Hach (Walters, 1991).

Calcium (Ca^{2+}) ions were titrated with ethylenediaminetetraacetic acid (EDTA)

which is used as a complexing-agent. Eriochrome Blue Black R was used as an indicator for the determination of the Ca^{2+} ion endpoint. The standard EDTA titrant of 0.01 M was prepared by measuring 3.7233 grams of EDTA, and dissolving the EDTA into one liter of distilled water. For analysis, the water samples were measured into 25-ml volumes. Next, 2.0 ml of 1 N NaOH solution were added to the samples to produce a pH of 12 to 13. Then 5 drops of Eriochrome blue black R indicator were added to the solution. The final step was to carefully add EDTA titrant, with continuous stirring to the proper end point. The calculation for calcium concentration is as follows:

$$mg\frac{Ca}{L} \quad \frac{A \quad B \quad 4008}{ml\ sample} \tag{20}$$

where

A = ml titrant for sample,

B = mg $CaCO_3$ equivalent to 1.00 ml EDTA titrant at the calcium indicator end point.

Alkalinity is the acid-neutralizing capacity of water and reflects the presence of carbonate, bicarbonate, and hydroxyl ions Within the pH ranges of most karst ground waters (Figure 11), only the bicarbonate ion makes a significant contribution to the alkalinity, and thus an acid titration is essentially a determination of HCO_3^- (White, 1988).

Alkalinity was determined with a digital titrator with a standard sulfuric acid solution to an end point pH, evidenced by the color change of a standard indicator

solution, based on Hach methods. Hach methods require filtration of a 50-ml water sample through .45 μm membrane filter. Phenolphthalein indicator and Bromcresol Green-Methyl were then added to the solution. The water samples were then titrated with a 1.6 N sulfuric acid solution connected to a J-hook, until the solution had a pH of 5.1, as indicated by a solutional color change from a green to a gray color (Walters, 1991). The precision of the above titration method is generally ± 0.01 mg/L.

An additional sample was then acidified with two ml of concentrated nitric acid and refrigerated, (Standard Methods 3500 - Ca D, Greenberg *et al.*, 1992), to preserve the sample for later magnesium concentrations analysis. Magnesium concentrations were measured with atomic absorption spectroscopy using the Varian SPECTRA AA-20 model at the Western Kentucky University water quality lab. Results from the water sample analysis were used to determine calcite saturation indices and carbon dioxide partial pressures.

The process of computing Pco_2 values and saturation indices for water samples can be tedious and time-consuming. Several computer programs have been developed precisely for this purpose, including PCWATEQ (Truesdell and Jones, 1974) and MINETEQ (Allison *et al.* 1991). The program KARSTSPEC (Groves, 1991), designed to calculate the Pco_2 and saturation indices associated with various carbonate and sulfate minerals in groundwater representative of karst aquifers, was used in the processing of the water samples collected from Charon's Cascade. KARSTSPEC calculates activity coefficients for the ionic species using the Debye-Hückel equation (Stumm and Morgan,

1981) and makes appropriate corrections for temperature and mass due to common ion pairs.

B. Crystal experiments. At the base of Charon's Cascade, a mineral weight loss experiment was conducted at various depths within the clastic sediment (the surface, 15 cm 30 cm, 60 cm, and 90 cm deep) (Figure 15). The mineral weight loss experiment had two purposes: (1) to determine processes, precipitation or dissolution, that are actually occurring to the limestone within the sediment, and (2) to compare actual limestone dissolution rates to theoretically predicted rates. Limestone pieces for the experiment were collected from a single large limestone block collected within the upper Ste. Genevieve Limestone from an area near Mammoth Cave National Park. The limestone block was cut into 43 six-sided tablets, approximately 0.4 by 2 by 12 cm. The samples were then prepared with methods similar to those used by Trudgill (1975) to remove the chemicals used in cooling the rock saws. Trudgill's (1975) cleaning procedure involved the use of four chemicals that were to be applied by rubbing the limestone pieces with one's fingers for ten seconds while the tablets were in the solution. The chemicals used for the procedure were applied in the following order: distilled water, dichloromethane, isopropyl alcohol, and acetone. After the samples were cleaned, the surface area of each tablet was measured, to a 50 th of an inch, using an engineering scale ruler.

Once the limestone tablets were measured the surface area was calculated, (Appendix F); the sides of the tablets were assumed to be flat for the purpose of surface area determination, although actual surface areas are likely to be larger due to small scale

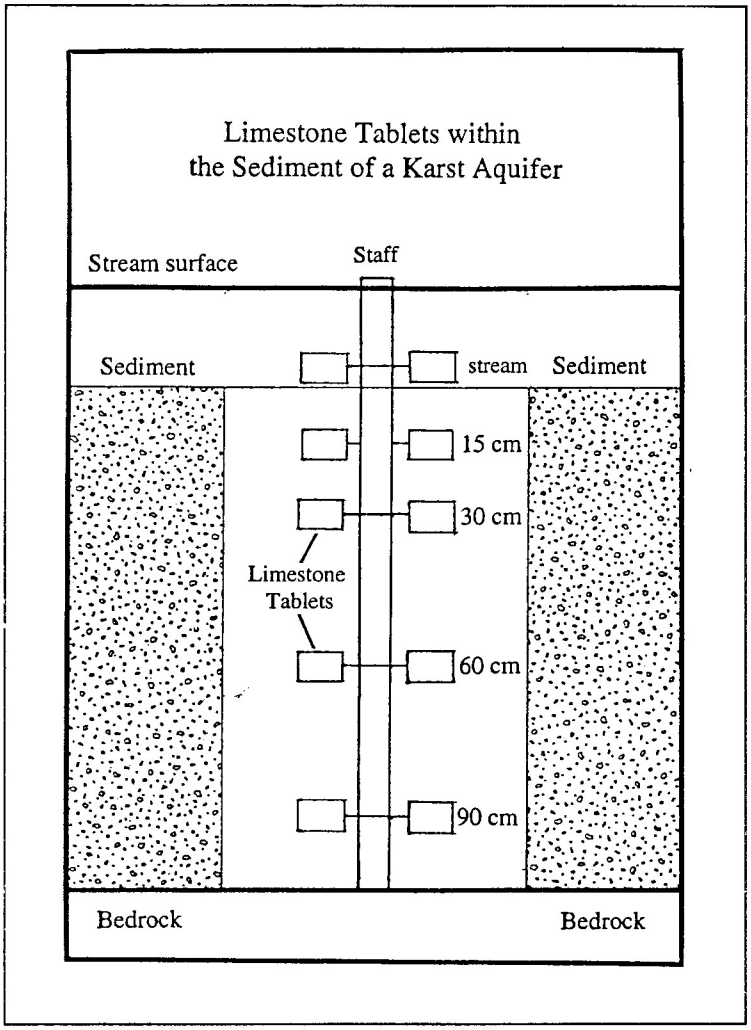

Figure 15. The placement of the limestone tablets at various levels within the clastic sediment at Charon's Cascade within Mammoth Cave.

roughness elements (Anbeek, 1979).

After the surface area was measured the limestone tablets were then placed into a heat vacuum oven for one week at 40 ^{0}C. The purpose of heating the tablets was to evaporate the water from the surface and the interior of the limestone tablets to establish a constant weight. After the limestone tablets were heated under vacuum for one week

the oven was turned off, but the vacuum was left on to allow the limestone tablets to cool to room temperature without allowing moisture to resettle on or within the tablet. After two days of cooling the limestone tablets were then removed from the oven and weighed to the nearest 0.0001 g (Appendix E).

The sample tablets were then placed within the cave sediment at depths of 90 cm, 60 cm, 30 cm, 15 cm and on the surface. To secure the limestone tablets in the sediment at known depths the tablets were fastened to four 122 cm galvanized steel angle braces. The limestone tablets were then secured to the aluminum wire with 30 lb test fishing line. Thirty-two tablets were placed within the sediment for 110 days, and seven samples were secured to the surface within the flowing stream (Figure 13), also for 110 days. Each angle brace was divided into five different levels with each level having two tablets. Placement of individual limestone tablets can be found within Appendix G. Every angle brace had a total of eight tablets within the sediment and two tablets on the surface. The top level was the surface stream, the second, third, fourth and fifth levels were 15, 30, 60, and 90 cm below the surface. In order to avoid contact between the limestone samples and the angle braces, aluminum wire was wrapped through the angle braces to create a 5 cm gap between the sample tablets and the angle braces.

In order to place the four angle braces into the sediment a capped 5 cm PVC pipe was used to bore a hole in the sediment in an attempt to cause minimal disturbance of the sediment. This process was achieved by first pushing an open, 7.62 cm diameter PVC pipe through the sediment, at the base of Charon's Cascade, to the desired depth.

Then a capped 5 cm PVC pipe was driven through the 7.62 cm PVC pipe creating a void space. The 5 cm pipe was then withdrawn from the sediment and the galvanized angle braces with the secured limestone tablets were placed into the void area. After the angle braces were secured, the 7.62 cm PVC pipe was quickly pulled out of the sediment allowing the sediment to collapse around the angle braces. After the sediment had collapsed around the angle braces the limestone tablets were left in the saturated sediment beneath the stream-bed for 110 days.

Upon removal of the limestone tablets from the sediment, the initial cleaning procedure was repeated. The samples were re-weighed, and the final weight was subtracted from the initial weight (Appendix H). A dissolution rate was then calculated by dividing the weight by the surface area and time of exposure of each sample giving a total weight loss per unit time per unit surface area. After the sample tablets were measured the rate that the limestone tablets dissolved was compared to determine what effect the clastic sediment had on limestone dissolution rates verses the dissolution that occurred within the active stream. The results were obtained by comparing the rates of limestone dissolution from within the active stream down through 90 cm of the clastic sediment. Theoretical dissolution rates determined from the water samples were then compared to the measured dissolution rates using a boundary-layer transport model.

Numerical flow modeling:

Determining the flow paths of the interstitial fluid within deposited sediments can

be difficult, because individual particles of the transported sediment are seldom spherical (Bouwer, 1978). As a result, when deposited under water, the particles usually come to rest on their flat side and are directionally orientated. Deposition of particles is directly dependent on sediment size, shape, orientation, and spatial packing. Particles deposited in flowing water may be tilted slightly upward in the direction of flow and may overlap. This arrangement is known as imbrication.

Imbrication may inhibit vertical mixing of fluid, because the path of water molecules flowing through imbricated material is more tortuous in vertical than in horizontal directions. Consequently anisotropy conducturities my result as the hydraulic conductivity k_z in a vertical direction will be less than k_x in a horizontal direction. Anisotropy can be caused not only by particle orientation but also by layering of materials with different k values, even though each layer itself may be relatively isotropic.

As a result of anisotropy, when the water molecules begin to flow along a particular flow line there may be little or no vertical mixing of the water. If no vertical mixing can occur, and the water flowing along a bedding plane line becomes saturated with calcite, no further limestone dissolution will be possible. Therefore, further limestone dissolution may occur only in an upward direction resulting in a paragenetic cave passage development.

A. Modeling. Fluid flow behavior within the sediment can be estimated with the application of simple quantitative flow model such as Darcy′ s law:

$$v = K\frac{dh}{dl} \tag{21}$$

where
K is the hydraulic conductivity [L T^{-1}],
v is the flow per unit area [L T^{-1}], and
dh/dl is the hydraulic gradient [unitless].

Measuring groundwater flow within a cave conduit presents a unique situation where the sediment in a cave conduit is being continuously recharged by a surface stream. This situation can make modeling of the hydraulic conductivity in a stream aquifer more difficult as a result from the stream-groundwater interactions. According to Sherry (1993), the equations used for modeling stream-aquifer interactions depend on the degree of hydraulic connection between the stream and the water table. For a stream bed such as Charon's Cascade, which is fully connected to the stream, the head within the sediment is identical to the water level in the stream, which is known.

In this experiment it was assumed that the limestone beneath the surface stream has negligible permeability and porosity. The limestone bed beneath the sediment could then be treated as an unconfined aquifer with a no flow-boundary condition along the bottom of the aquifer. The assumption that Bouwer's (1978) particle orientation theory will hold true for the particles deposited by the River Styx will allow the use of a variation of Darcy's law for measuring the hydraulic conductivity.

The hydraulic conductivity of the sediment was measured with use of a constant-head permeameter device (Figure 16) which can be used for noncohesive sediments-

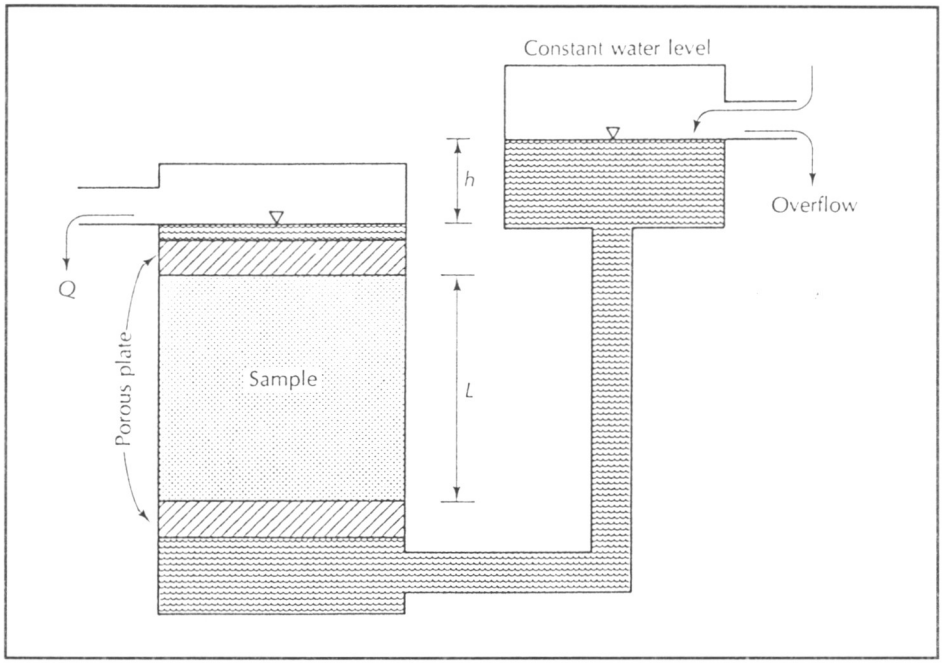

Figure 16. Constant-head permeameter apparatus (Source: Fetter, 1992).

such as sand, silt, rocks, and gravels (Fetter, 1992). A cell with an overflow area provides a supply of water at a constant head, which also allows water to move through the sample at a steady rate. The hydraulic conductivity of the sample can then be determined with a simple transformation of Darcy's law:

$$K = \frac{VL}{Ath} \tag{22}$$

where

V is the volume of water discharging in time t [L^3],

L is the length of the sample [L],

A is the cross-sectional area of the sample [L^2], and

h is the hydraulic head [L].

To estimate the velocity of the interstitial fluid movement within the sediment the hydraulic conductivity of the sediment was measured at the base of Charon's Cascade. The Hydraulic conductivity of the sediment was measured through the collection of push core samples taken from the area where the limestone tablets were placed within the sediment. The core samples were collected with a 7.62 cm diameter by 122 cm PVC pipe that was pushed into the sediment, capped, and removed in an attempt to minimize disturbance of the sediment. The PVC pipe was then manually transported back to Western Kentucky to measure the hydraulic conductivity. The hydraulic conductivity was measured with the use of a constant-head permeameter apparatus (Figure 15). Once the hydraulic conductivity was measured, the effective porosity could then be determined. Effective porosity (n_e) can be defined by

$$n_e = (n)(epf) \tag{23}$$

where

n is the porosity [unitless], and

epf, the effective pore fraction, is the porosity available for fluid flow [unitless].

Porosity can be computed from the relationship

$$n \quad [1 \quad (\frac{\rho_b}{\rho_d})] \tag{24}$$

where

ρ_b is the bulk density of the aquifer material [M L^{-3}], and

ρ_d is the particle density of the aquifer material [M L^{-3}].

Once the hydraulic conductivity and the effective porosity are determined the average linear velocity of the water moving through the sediment can be found by the equation

$$V_x = \frac{Kdh}{n_e dl} \tag{25}$$

where

V_x is the average linear velocity [L T^{-1}], and

dh/dl is the hydraulic gradient [unitless].

After the hydraulic conductivity and the effective porosity were measured the samples were prepared for a particle-size analysis following the step-by step procedures found in Standard Methods (Klute, 1985). Particle-size analysis (PSA) is a measurement of the size distribution of individual particles in a sediment sample and is among the oldest of the soil tests (Liu and Evett, 1990). One way of measuring sand, silt, and clay size particle distribution within a sediment sample is by combining the hydrometer and sieving method together. The hydrometer method depends fundamentally upon Stoke's Law, which for the hydrometer may be written as

$$X = \theta t^{-\frac{1}{2}} \tag{26}$$

where

θ is the sedimentation parameter and is a function of the hydrometer settling depth, solution viscosity, and particle and solution density. θ can be defined as the following:

$$\theta = 1000(Bh')^{\frac{1}{2}} \quad (27)$$

where

B is a solution viscosity parameter dependent on Stoke's Law, defined as

$$B = \frac{30\eta}{[g\ (\rho_s - \rho_l]} \quad (28)$$

where

η is the fluid viscosity in poise [$M\ L^{-1}\ T^{-1}$],

g is the gravitational constant [$L\ T^{-2}$],

ρ_s is the soil particle density [$M\ L^{-3}$], and

ρ_l is the solution density [$M\ L^{-3}$].

The effective hydrometer depth is h' [L] is as follows:

$$h' = -.164R + 16.3, \quad (29)$$

where R [L] is the uncorrected hydrometer reading.

Samples were prepared for the hydrometer test by mixing 40 g of sediment sample with 50 g/L of sodium hexametaphoshate (HMP) in a standard blender for 7 minutes. Sodium hexametaphoshate is a deflocculent which causes aggregated particles to separate into their individual particles while in solution. After the sediment and HMP were mixed into a solution, the solution was then poured into a one liter cylinder and mixed with deionized water. The cylinders were capped and then turned end over end 20 times to disturb the settled sediments. Hydrometer readings were then taken at the 30 sec, 1 min, 3 min, 10 min, 30 min, 60 min, 90 min, 120 min, and 1440 min intervals. The results from the Hydrometer can be found within Appendix I and J.

After the hydrometer tests were completed the solutions were then poured through a number 230 sieve, opening size 0.06 mm, oven dried at 105 °C and re-weighed. Once the samples were re-weighed, the remaining sand size particles were mechanically sieved following ASTM D 422-63 (Klute, 1985); results can be found in Appendix K. The results were reported in the form of a grain-size distribution curve, and in tabular form, providing percentages passaging through various sieves sizes (Appendix L).

B. Theoretical dissolution rates. Several theoretical dissolution rate equations based on the chemistry of water samples have been developed, including the well known rate expression of Plummer *et al.* (1978):

$$Rate = k_1 a_{H^+} + k_2 a_{H_2CO_3} + k_3 a_{H_2O} - k_4 a_{Ca^{2+}} a_{HCO_3^-} . \qquad (30)$$

The rate is given in units of millimoles per centimeter square per second. The first term describes the rate of reaction of calcite with protons. The second term describes the reaction of calcite with carbonic acid and contains the dependence of the reaction rate on carbon dioxide pressure. The third term describes the dissolution of calcite in water (White, 1988). The temperature dependence of the forward reaction rate constants of the Plummer-Wigley-Parkhurst model were determined as follows (Plummer *et al.*, 1978):

$$\log k_1 = 0.198 - \frac{444}{T}, \tag{31}$$

$$\log k_2 = 2.84 - \frac{317}{T}, \tag{32}$$

$$\log k_3 = -5.86 - \frac{317}{T}, \tag{33}$$

where T is temperature in degrees Kelvin.

The back-reaction terms has a complicated dependence on all of the other variables,

$$k_4 = \frac{K_2}{K_{cal}} \left[k'_1 + \frac{1}{a_{H^+}} \left(k_2 a_{H_2CO_3} + k_3 a_{H_2O}\right)\right], \tag{34}$$

where

k' is k_1 * 10 (Plummer *et al.*, 1978), and

K_2 and K_{cal} are temperature dependent equilibrium constants.

To predict the amount of limestone dissolution that may be occurring beneath the clastic sediment a theoretical dissolution rate equation was developed based on mass transfer rate equations for a three dimensional flat plate suspended within a porous medium. The theoretical dissolution rate equation was based on several assumptions: (1) the dissolution of calcite ions from the solid phase was transport limited, (2) the thickness of the concentration boundary layer is a constant for the length of the plate.

The first process in understanding a mass transfer reaction is to determine the flow conditions of the fluid. If a fluid of species molar concentration C_B (calcium) flows over a surface at which the species concentration is maintained at some value $C_A \neq C_B$, transfer of the species by convection will occur. The mass transfer rate is modeled by the diffusion of calcium from the mineral surface into the fluid. The rate of mass transfer of Ca^{2+} from the mineral surface is given by (Incropera and De Witt, 1985)

$$R = h_m(Ca^{2+}_A - Ca^{2+}_B) \quad (35)$$

where

R is the dissolution rate of limestone in [M L^{-2} T^{-1}],

Ca^{2+}_A is the calcium concentration at the mineral surface [M L^{-3}],

Ca^{2+}_B is the mean calcium concentration across the flat plate [M L^{-3}], and

h_m is the convective mass transfer coefficient [L T^{-1}].

Ca^{2+}_A is a function of temperature and the partial pressure of carbon dioxide, and

can be solved using carbonate equilibrium relationships (White, 1988; Palmer, 1991).

$Ca^{2+}{}_B$ is the calcium concentration obtained from the water sampling analysis within the clastic sediment. The central task when developing a mass transfer equation is to find an appropriate value for the convection coefficient h_m. To determine the transport of calcium over a flat plate through a porous medium several factors need to be considered, including (1) the concentration gradient from the surface to the boundary layer and (2) diffusion of calcium from the surface through the boundary layer. The convection coefficient can be estimated by

$$h_m \quad \frac{Sh\ \delta_{Ca}}{L} \tag{36}$$

where

Sh is the dimensionless Sherwood Number [unitless],
δ_{Ca} is a diffusion coefficient for the calcium ion [$L^2\ T^{-1}$], and
L is the length of the individual limestone tablet placed within the sediment [L].

The Sherwood Number represents the ratio of convective to diffusive mass transport and is analogous to the Nusselt Number of heat transfer theory (Incropera and De Witt, 1985). Values for Sh depend on flow condition and conduit geometry and have been theoretically and experimentally determined for a number of circumstances. The Sherwood Number may be described as the following:

$$Sh = 0.664\ Re^{\frac{1}{2}}\ Sc^{\frac{1}{3}} \tag{37}$$

where

Re is the dimensionless Reynolds number and is equivalent to the ratio of the inertial and viscous forces [unitless], and

Sc is the dimensionless Schmidt number and is equivalent to the ratio of the momentum and mass diffusivities [unitless].

The Reynolds number is determined using the following equation:

$$Re = \frac{VL}{\gamma} \tag{38}$$

where

V is the average linear velocity [L T^{-1}],

L is the pore diameter of the clastic sediment [L], and is estimated by using median grain size [Freeze and Cherry, 1979], and

γ is the fluid kinematic viscosity [L^2 T^{-1}].

The Schmidt Number (Sc),

$$Sc = \frac{\gamma}{\delta_{Ca}}, \tag{39}$$

is a dimensionless quantity that expresses the ratio between momentum transfer and mass transfer by diffusion and is analogous to the Prandtl Number of heat transfer theory.

Once all of the groundwater samples have been analyzed the data can be used in the above equations to estimate a dissolution rate for the limestone within the clastic sediment. The theoretical dissolution rates predicted for the limestone tablets within the clastic sediment were then compared to the measured dissolution rates.

Qualitative sample analysis

Before the limestone blocks were placed within the sediment the purity of the original limestone was established by measuring the amount of insoluble residue within the limestone. This procedure was accomplished by grinding several grams of the limestone block into a fine powder. The limestone powder was weighed and then dissolved in 38% hydrochloric acid. After 24 hours in the acid the remaining solution was then filtered under vacuum with hydrochloric acid and distilled water through a 45 μm filter paper.

Particles that did not dissolve were trapped on the filter paper; those are the insoluble residue. Common insoluble residue found within limestone, often quartz type material, can be found in any combination of size sand, silt, or clay. The insoluble residue trapped on the membrane filter was oven dried at 105^{0}C, allowed to cool, and then weighed. The insoluble weight was then divided into the original weight to determine the purity of the limestone samples that were being used for the crystal weight loss

experiment. Purity of the limestone samples can be found in Appendix C. The insoluble residue was then carbon coated and placed under a scanning electronic microscope (SEM) for a closer examination of the insoluble residue (Figure 17). The majority of the

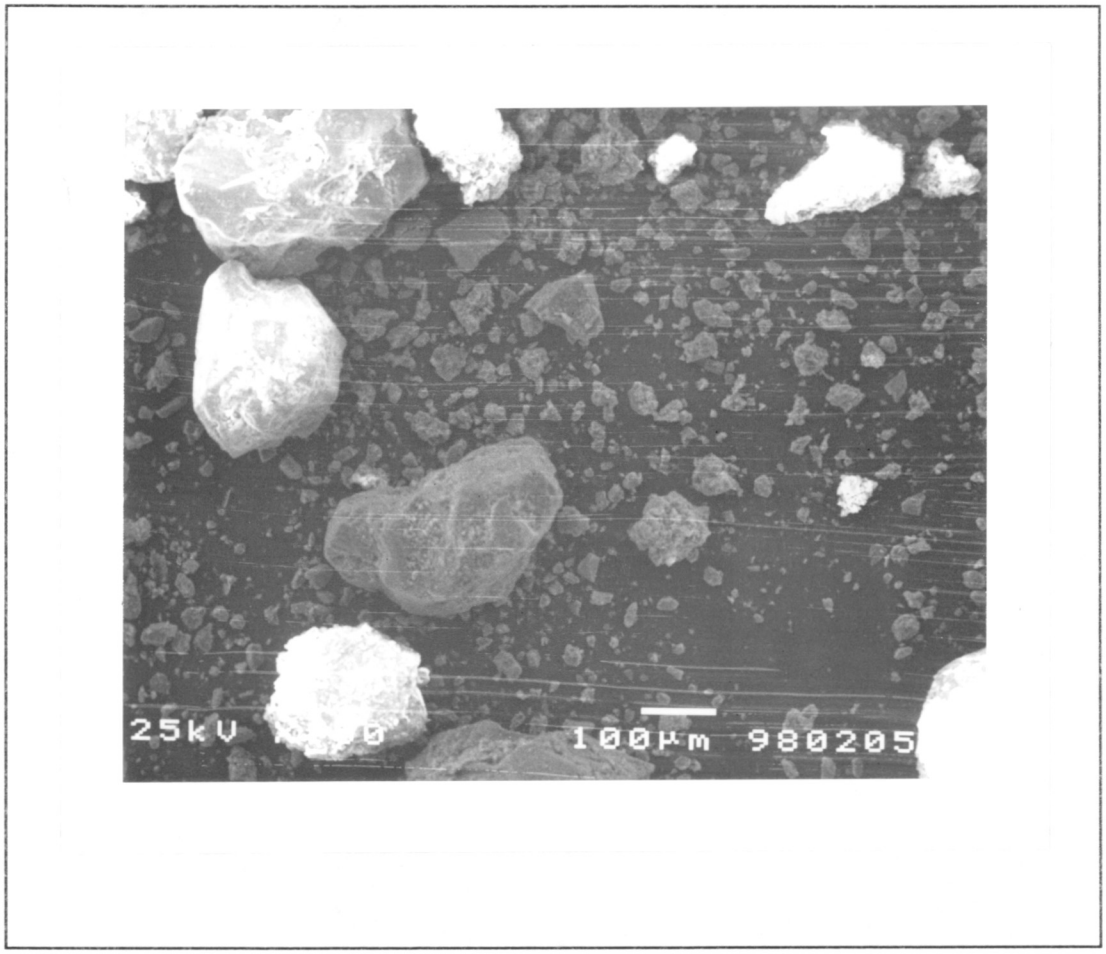

Figure 17. Insoluble residue from the limestone tablets used in the dissolution experiment as seen under the scanning electron microscope.

sediment from Figure 17 is quartz of different sizes, sand, silt, and clay. Viewing the sediment under SEM was not advantageous for this study. Microbial activity or organic

material were not discernible under SEM, and the use of SEM in further similar research studies is not recommended.

Sediment core sampling

Sediment core samples were collected from Charon's Cascade and the upper end of the River Styx. The core samples were collected with a 3.2 cm diameter by 89 cm PVC pipe. A coupler and a 25 cm joint pipe were added on the top of each pipe. The PVC pipes were then driven down into the sediment until the pipes were full. After the pipes were filled with the sediment a cap was placed over the pipes to create a vacuum. The pipes were then pulled out of the sediment, and the bottom of the pipe was capped off. To create a solid core sample with little or no void space, the 25 cm joint pipe was removed, and a new cap was then placed on the top. After the sediment core samples were removed from Mammoth Cave, the caps were removed so the samples could be air-dried. After the sediments were dried the pipes were cut open using a table saw to profile and classify the sediments. The sediment core samples were profiled with a Munsell color chart and classified by the criteria set by the U.S. Department of Agriculture for field methods of determining soil texture classes (Brady, 1990). The results from the soil classification can be found within Appendix D. Sediment profiles may be important in understanding interstitial fluid movement within the sediment and the chemical reactions that may be occurring between the water, rock, microbial activity, and the sediment.

CHAPTER V

RESULTS AND DISCUSSION

Results

A. Interstitial fluid chemistry

The primary purpose of this research has been to understand the carbonate chemistry of the interstitial fluids within the sediment beneath the flowing stream of Charon's Cascade. With this information, it is then possible to evaluate the water rock interaction within the sediment and, ultimately, what impact this sediment is having on cave passage development.

Water samples were collected from the surface stream, as well as from 15, 30, 60, and 90 cm beneath the stream bed. The water samples were then analyzed to determine the pH, temperature, specific conductance (spC), calcium, magnesium, and bicarbonate concentrations. Averages from the water samples collected at Charon's Cascade during the experiment are shown in Table 1; complete data are listed in Appendix A.

The chemical data measured from the active stream and the interstitial fluids were first used to calculate the CO_2 pressure and saturation index with respect to calcite and dolomite. The mean values from the experiment are shown in Table 2; complete data are listed in Appendix B. Carbon dioxide pressures are reported in atmospheres and in the

Table 1. Averages from the water samples collected at Chaon's Cascade

Location	pH	t (° C)	spC (µs)	Ca^{2+} (mg/L)	Mg^{2+} (mg/L)	HCO_3^- (mg/L)
stream	7.76	12.5	211	42	3.1	61
15 cm	7.06	12.1	323	53	7.2	134
30 cm	7.03	12.0	322	56	7.1	115
60 cm	6.98	11.9	326	57	7.4	136
90 cm	6.96	11.8	353	56	7.1	125

ratio of the measured pressure to atmospheric background levels.

Table 2. Mean calcite saturation indices and Pco_2 concentrations at Charon's Cascade.

Location	SI calcite	SI dolomite	Pco_2 (atm)	Pco_2 ÷ atm background (350 ppm)
stream	-0.385	-1.747	$9.1x10^{-4}$	2.6
15 cm	-0.720	-2.241	$8.5x10^{-3}$	24.1
30 cm	-0.844	-2.429	$7.2x10^{-3}$	20.6
60 cm	-0.829	-2.388	$9.4x10^{-3}$	26.7
90 cm	-0.896	-2.532	$8.9x10^{-3}$	25.5

The most striking result is that CO_2 pressures within the interstitial fluids were generally an order of magnitude higher than those for the water in the active stream. The active stream was on average 2.6 times higher than atmospheric background, and the

CO_2 pressure within the sediment ranged from about 20 to 27 times background- with no clear increasing or decreasing trends with depth.

Since the ability of a fluid to dissolve limestone is directly related to its CO_2 pressure, it is not surprising that the calculated calcite saturation indices within the sediment fluids are substantially more negative than those for the stream water. Generally, water within the sediment was about three times more undersaturated, again with no clear trends with depth. These values suggest that the waters within the sediment should be capable of dissolving limestone, possibly, at a faster rate than the stream waters of Charon's Cascade.

Although the waters were found to be undersaturated, and thus dissolution is predicted, dissolution of limestone may or may not actually be occurring. Dissolution rates are not only impacted by the chemical conditions, but are also impacted by the flow conditions of the fluid with which these minerals are in contact. For example, if fluid velocities within the sediment are sufficiently low that the reaction products are very slowly removed from the vicinity of the mineral surface, the possibility exists that a region of saturated fluid can accumulate at the sediment/fluid interface. In this case saturated fluids are in contact with the mineral rather than the undersaturated fluids which were generally found to occur within the sediment. The hydraulic conditions and the flow velocities of the fluids from this experiment can be found in Table 3.

Table 3. Hydraulic conductivity of the sediment at Charon's Cascade

Depth from active stream	Hydraulic gradient	Effective porosity (%)	Hydraulic conductivity (cm s^{-1})	Average linear velocity (cm s^{-1})
0 to 30 cm	0.01	0.29	3.2×10^{-3}	1.29×10^{-4}
30 to 60 cm	0.01	0.27	2.8×10^{-3}	1.21×10^{-4}
60 to 90 cm	0.01	0.39	2.2×10^{-4}	6.60×10^{-6}

The velocities of the fluid moving through the porous medium are significant when trying to understand the fluid's ability to transport dissolved limestone from the system. The average linear velocities of the waters that flow through the sediment at Charon's Cascade varied. Near the active stream the fluid velocities were about 1.3×10^{-4} cm s^{-1}, with an increase in depth beneath the active stream the fluid velocities decreased to approximately 6.6×10^{-6} cm s^{-1} The decrease in the average linear velocity with depth follows the overall trend of the sediment core profiles which typically had coarser size particles near the top and finer size particles near the bottom.

B. Measured dissolution rates

Limestone dissolution depends both on the chemistry and the flow conditions of the fluid. Although the water chemistry indicates that limestone dissolution should occur, that indication does not necessarily mean that limestone dissolution will proceed within

the sediment. To simulate what my be occurring to limestone rocks beneath the sediment at Charon's Cascade limestone dissolution rates were directly measured by placing limestone samples of known mass and surface area within the active stream and into the sediment at the same levels from which the water samples were collected.

Each angle brace was divided into five levels with each level having two limestone samples. The limestone samples for this experiment were in contact with the fluids from Charon's Cascade for 110 days. During the study period the blocks remained saturated within the sediment beneath the stream bed, and the whole passage was actually flooded at various times (Figure 18).

The base of Charon's Cascade is composed of a complex stratigraphy of intermixed sand, silt, and clay (Appendix D). As a result of the stratigraphy minimal hydrologic conditions may exists, therefore limiting the fluids ability to actively dissolve and transport dissolved calcite ions outside of the boundary layer. No weight loss or calcite percipitation may occur to an individual limestone sample used in this experiment even though the fluid chemistry suggests that dissolution should occur. The results from this experiment can be found Table 4, and the weight loss can be found in Appendix L.

In every case, the limestone samples that were placed within the active stream and the clastic sediment did lose weight. However, the rate of limestone dissolution varied for the limestone samples that were placed within the active stream, and those which were placed within the sediment. For the limestone samples that were placed with stream dissolution rates that varied from 11.85 to 39.51 g m^{-2} yr^{-1}, and the dissolution rates for

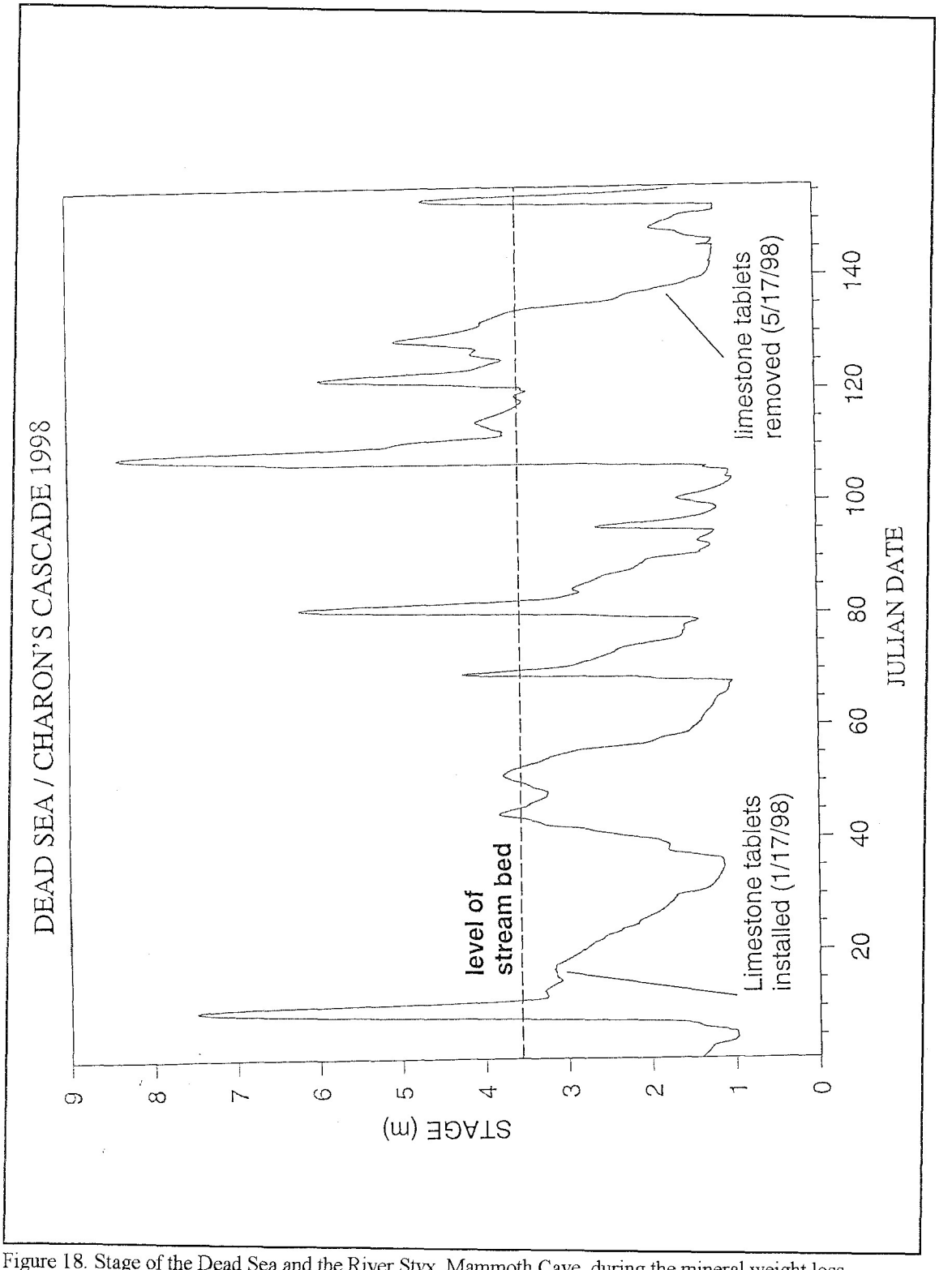

Figure 18. Stage of the Dead Sea and the River Styx, Mammoth Cave, during the mineral weight loss experiment.

Table 4. Dissolution rates of individual limestone tablets (g m^{-2} yr^{-1}).

Sample Depth	rod 1	rod 1	rod 2	rod 2	rod 3	rod 3	rod 4	rod 4
surface		17.19	22.69	39.53			15.86	11.85
15 cm	7.89	5.14	14.13	13.21	18.45	17.62	8.56	11.45
30 cm	3.10	4.61	11.32	21.90	6.30	6.14	2.60	4.05
60 cm	8.33	13.37	12.28	14.24	15.86	4.81	11.32	5.87
90 cm	6.11	7.33	7.63	7.70	1.36	6.60	6.30	0 .83

the samples that were placed within the clastic sediment varied from 0.83 to 21.90 g m^{-2} yr^{-1}, again with no clear trend with depth.

Since the rate of limestone dissolution varied for each individual level it is difficult to determine the overall impact that the sediment has on dissolution rates. To obtain an understanding of the overall process that occurred an average rate oflimestone dissolution was then determined for each level. The arithmetic mean of the data set can be greatly impacted by large variations within the data set. To measure the variability of the mean the standard deviation and coefficient of variation of the data set were also determined. The results of theses calculations are presented in Table 5; the total number of samples is n = 37.

Table 5. Descriptive statistics of measured dissolution rates

Sample Depth	Mean dissolution rate ($g\ m^{-2}\ yr^{-1}$)	Standard Deviation ($g\ m^{-2}\ yr^{-1}$)	Coefficient of variation (%)
Surface	21.42	10.82	50.51
15 cm	12.05	4.71	39.09
30 cm	7.50	6.51	86.80
60 cm	13.60	4.01	29.49
90 cm	5.48	2.78	50.55

The most striking aspect is that the limestone dissolution rates within the sediment, even though they were slower, were comparable with those in the active stream. Even though the fluid chemistry of the active stream had calcite saturation indices closest to equilibrium, the limestone dissolution rates were the fastest overall. The indication is that the flow conditions impact dissolution.

In most cases, it is not convenient to directly measure limestone dissolution rates. It would be much simpler to analyze water samples and then use a theoretical limestone dissolution rate equation to determine passage development. Since most theoretical dissolution rates equations were developed under ideal laboratory conditions, concerns about the accuracy of these equations under natural conditions have been raised (Morse, 1983 and Dreybrodt, 1992).

To determine if it was possible to predict limestone dissolution rates at Charon's Cascade two different theoretical dissolution rate equations were used. For the fluid

flowing along the base of Charon's Cascade the rate expression of Plummer *et al.* (1978) was used. For the interstitial fluid beneath the base of Charon's Cascade a dissolution rate equation was developed from mass transfer equations. Results are shown in Table 6.

Table 6. Predicted limestone dissolution rate in g m^{-2} yr^{-1} for individual limestone tablets within the sediment, and the active stream.

sample depth	rod 1	rod 1	rod 2	rod 2	rod 3	rod 3	rod 4	rod 4
surface	2008	2008	2008	2008	2008	2008	2008	2008
15 cm	0.0076	0.0075	0.0062	0.0073	0.0074	0.0078	0.0066	0.0052
30 cm	0.0053	0.0049	0.0049	0.0051	0.0057	0.0053	0.0061	0.0052
60 cm	0.0024	0.0021	0.0020	0.0022	0.0022	0.0021	0.0021	0.0017
90 cm	0.0003	0.0002	0.0003	0.0003	0.0003	0.0003	0.0003	0.0003
mean								
surface	2008							
15 cm	0.0069							
30 cm	0.0053							
60 cm	0.0021							
90 cm	0.0003							

An interesting result is that the rate of predicted dissolution in the active stream was, in some cases, seven orders of magnitude faster than the predicted limestone dissolution rates within the sediment. Variation between the two different theoretical

dissolution rate equations can be determined. Of major importance is determinig the ability of the theoretical dissolution rate equation to accurately predict limestone dissolution that should occur under natural conditions. The ultimate goal is to use a theoretical dissolution rate equation, depending on the environmental conditions, to accurately determine how a cave passage has developed and will continue to do so.

It is important to determine the success of the theoretical dissolution rate equations, and to do so the measured dissolution rate of each individual limestone sample was divided by the predicted rates. Results from this calculations are presented in Table 7.

Table 7. A comparison of the measured dissolution rates divided by the predicted rates

Sample Depth	rod 1	rod 1	rod 2	rod 2	rod 3	rod 3	rod 4	rod 4
surface		8.5e-3	0.011	0.019			7.8e-3	5.8e-3
15 cm	1031	688	2264	18121	2470	2244	1290	2182
30 cm	586	952	2335	4323	1116	1162	429	783
60 cm	3516	6480	6077	6750	7356	2332	5483	3529
90 cm	21607	31183	25307	24382	5234	22389	21373	2812

Overall, the variations between the predicted and the measured limestone dissolution rates greatly varied. The differences between the Plummer *et al.* rate expression for fluids within the active stream ranged from 50 to 180 times faster than the

measured limestone dissolution rates. A larger range of variation occurred between the predicted and measured limestone dissolution rates within the clastic sediment. The differences between the mass transfer dissolution rate equation for the interstitial fluids ranged from 429 to 31,183 times slower than the measured rates.

Discussion

Paragenesis assumes that the clastic sediment within a cave passage inhibits limestone dissolution from occurring, and that dissolution is focussed on the unprotected ceiling. However, quantitative evaluation of the impact of cave sediments on dissolution rates has received little attention. It is well known that natural waters are often undersaturated with respect to calcite and have the ability to dissolve limestone. The chemistry of fluid flowing from Charon's Cascade is similar to other waters flowing within Mammoth Cave System. The most striking results were the differences that were found within the interstitial fluid beneath the active stream.

According to Table 1, the active stream solution had the highest average pH of 7.76, and a calcite saturation index nearest equilibrium. The pH of the solution within the clastic sediment was, on average 7.01, lower than the active stream, with saturation indices further away from equilibrium than the active stream. According to Table 2, the water chemistry of the active stream had the lowest Pco_2 value of 2.6 times atmospheric background. Within a short distance beneath the active stream the interstitial fluid Pco_2 values rapidly increased, on average, from 2.6 to 20 to 27 times atmospheric background.

The differences in the water chemistry of the fluid within the active stream and the interstitial fluids probably result from microbial decomposition of organic matter which releases CO_2. The increase in CO_2, within the interstitial fluid causes an increase in the Pco_2 and a decrease in the pH.

Although the interstitial fluid was undersaturated with respect to calcite, the meaning is not that the limestone within the non-carbonate sediment will dissolve (Curl, 1965; Plummer and Wigley, 1976; Plummer *et al.*, 1978 and 1979; Dreybrodt, 1981; Palmer, 1991). All of the limestone tablets for this experiment did dissolve, but they dissolved at different rates. Overall, limestone dissolution rates were faster within the active stream than within the clastic sediment, even though the active stream was closer to equilibrium than the interstitial fluid. The indication is that the flow conditions impacted dissolution, even though the saturation indices were lower in the sediment. Thus the meaning is not only does fluid chemistry, but also flow conditions have an impact on limestone dissolution rates and conduit development. The volume and classification of the non-carbonate sediment within a conduit system, and the conduit's ability to transport sediment may be important when trying to understand conduit development.

Within the clastic sediment the overall rate of limestone dissolution decreased with an increase of depth beneath the active stream. The decrease in dissolution rates coincided with an increase in depth beneath the clastic sediment. The decrease in dissolution rates by depth within the clastic sediment may be related to the velocity of the

fluid moving through the sediment.

Based on the sediment core samples collected from the base of Charon's Cascade some general trends can be determined (Appendix E). Overall, the sediments ranged from pale to a reddish brown with finer silt size particles found near the bottom and larger coarse sandy particles found near the top. The lack of clay found within the sediment is very important to the hydrogeologic conditions of the sediment. The lack of clay means the sediments are permeable enough to readily transmit water. Water movement is important for removal of calcium ions from the limestone surface out into the solution.

Based on the chemistry and flow conditions of the water, two separate theoretical limestone dissolution rate equations were used to determine if it was possible to predict the rate of limestone dissolution that occurred at the study site. The Plummer *et al.* (1978) equation was chosen to predict limestone dissolution rates within the active stream. It was found that the PWP rate equation overpredicted the amount of dissolution from 50 to 180 times the measured dissolution rate. The differences in the rate of dissolution from the measured and predicted equation may be contributed to different possibilities: abrasion, lithology, addition of foreign ions.

Abrasion is the frictional disintegration of limestone by the clastic sediment. During flood events (Figure 18) the fluid velocity may have moved the clastic sediment causing abrasion to occur to the limestone tablets located on top of stream bed. Abrasion was not factored into the Plummer *et al. (1978)* equation and it may be an important, but

little studied, process in passage development.

Differences in lithology included porosity and purity. Porosity is a function of grain size and arrangement (packing), and purity depends on the amount of insoluble material present (Rauch and White, 1977). The higher the effective porosity the farther into the crystal the water can penetrate, meaning that there a greater surface area on which the reaction can occur. As the purity of the limestone decreases the conditions become less like the experimental conditions from which the equations were derived. The purity of limestone samples that were used in this experiment were roughly 97% pure calcite (Appendix C). Natural waters are rarely pure and are commonly found to have foreign ions (Drever, 1997). Morse (1983) and Dreybrodt (1992) have found that foreign ions, possibly phosphate, may affect calcite dissolution rates.

Water samples used for predicting the theoretical dissolution rates showed very little variation in the chemistry. However, the chemistry was determined from five water samples. Data were not collected continuously nor was it possible to collect data under flood conditions (Figure 18). Based on the chemistry of the water samples, being near equilibrium with respect to calcite, the Plummer *et al.* (1978) equation may not have produced more accurate results even with continuous data. Others have shown that the Plummer *et al* (1978) equation tends to overpredict dissolution rates for limestone in waters near equilibrium.

To predict limestone dissolution rates within the clastic sediment a theoretical dissolution rate equation was developed from mass transfer theory. This equation

greatly underpredicted limestone dissolution rates from 429 to 31,183 times the measured rates. The theoretical mass transfer dissolution rate equation was not adequate for predicting limestone dissolution rates that occur beneath the clastic sediment of an active stream. The mass transfer equation may have underpredicted the rate of dissolution for various reasons: abrasion, limited number of water samples, and an underestimate of the very rough estimate of the velocity coefficient (h_m).

During flood events (Figure 18) it may have been possible that the large volume of water may have partly scoured the base of Charon's Cascade resulting in the clastic sediment causing abrasion to occur to the limestone tablets located within the clastic sediment. Abrasion was not factored into the mass transfer equation, and it may be an important, but little studied, process in passage development.

Water samples used for predicting the theoretical dissolution rates showed very little variation in the chemistry. However, the chemistry was determined from five water samples. If data sampling were continuous the chemistry of the water samples may have had a larger variation, and a more accurate theoretical analysis could have been achieved.

The velocity coefficient is basically the controlling parameter for the mass transfer equation, and it still needs further adjustment. A possible error in the velocity coefficient may arise from an underestimation of the rate that calcium ions can be transported out of the diffusion boundary layer. It was probably incorrectly assumed that the dissolution of calcite within the clastic sediment was adversely impacted by the fluid's inability to

transport calcium ions outside of the boundary layer. If the interstitial fluid is able to readily transport calcium ions, limestone dissolution rates may proceed at a rate faster than that predicted by the theoretical dissolution rate equation. Further adjustment needs to be made to the velocity coefficient before accurate predictions can be made regarding limestone dissolution rate processes within the clastic sediment.

The most important result is that the interstitial fluid beneath an active cave stream has the ability to readily dissolve limestone. Therefore, passages may be forming beneath, and breakdown blocks dissolving within, the sediment. In this study the researcher presents evidence that the River Styx passage near Charon's Cascade has not formed as a result of paragenesis.

CHAPTER VI

CONCLUSIONS AND FURTHER RESEARCH

Conclusions

The chemistry of the water samples, taken within the cave stream and sediment, varied from near calcite equilibrium within the active stream towards more undersaturated conditions with depth beneath the aquifer stream. The water chemistry of the active stream was found to have Pco_2 values, on average, of 2.6 times atmospheric concentrations. The interstitial fluid was also found to have elevated Pco_2 values, averaging 20.0 to 27.0 times atmospheric concentrations. The fluid chemistry suggests that limestone tablets located within the sediment should dissolve at a faster rate than the sample tablets located within the stream. However, the fluid velocities within the sediment were four orders of magnitude slower than the surface stream limiting the fluid's ability to remove calcium ions.

However, dissolution occurred on every limestone tablet used in this study, but the rates of limestone dissolution varied. The measured rates varied inversely with the calcite saturation indices determined from the water chemistry. Overall, the fastest rate of limestone dissolution occurred within the active stream, and the rate of dissolution slowly decreased with an increase of depth through the clastic sediment. The average

limestone dissolution rate within stream bed was 21.41 g m^{-2} yr^{-1} (Table 5), and, on average, at 9.6 g m^{-2} yr^{-1} (Table 5) within the sediment. If we assume that the previous dissolution rates remain as constants for approximately one million years the passage would be enlarged by roughly 10.5 meters in an upwards direction, and widened roughly 4.8 meters. These are very reasonable numbers based on the present age and dimensions of some passages within the Mammoth Cave area.

Paragenesis suggests that limestone dissolution will not occur beneath the clastic sediment of a karst aquifer. It was determined that at the base of Charon's Cascade the clastic sediment did not inhibit limestone dissolution from occurring nor did it significantly decrease the rate of dissolution. These results provide evidence that some of Mammoth Cave's passages may not have formed as a paragenetic processes, but rather that passage development occurred as a combination of vadose entrenchment and aggradation. For example, when large pieces of limestone fall from the ceiling, in a process known as breakdown, and are buried within the clastic sediment, dissolution may still occur, eventually removing the rock from the passage.

To determine if passage development could be predicted, two different dissolution rate equations, (Plummer *et al.*, 1978 and a mass transfer equation) based on the chemistry and flow conditions of the waters, were compared to measured limestone dissolution rates at the study site. Within the active stream limestone dissolution rates occurred 50 to 180 times slower than those predicted by the water chemistry, and the theoretical dissolution rate equation. The theoretical mass transfer dissolution rate

equation greatly underpredicted, from 429 to 31,183 times, the amount of dissolution that occurred within the clastic sediment. Therefore the theoretical dissolution rate equation developed from mass transfer equations needs further refinement before it can be used to accurately predict limestone dissolution rates that occur within the clastic sediment at Mammoth Cave.

Even though dissolution of dolomite was not directly measured, the results obtained from the calcite dissolution experiment should be directly applicable to areas where dolomite is present. Although dolomite is less soluble than calcite the interstitial fluid was further away from equilibrium with respect to dolomite. Saturation indices of the interstitial fluid for dolomite were, on average, (Table 2) -2.4. Since calcite dissolution occurred within the sediment at base of Charon's Cascade, dolomite dissolution should occur at rates comparable to any dolomite within a aquifer stream.

Results from this study have important implications for understanding rates and geometries of conduit evolution within karst aquifers. Not only is it important to understand limestone dissolution that occurs along the ceiling, but also understanding how the non-carbonate sediment impacts passage development may be crucial when developing aquifer models.

Recommendations for further research

This attempt was a first attempt at trying to understand what effect the clastic sediment in a cave has on dissolution rates of the surrounding limestones. The results

of this study showed that at the base of Charon's Cascade limestone dissolution took place beneath the clastic sediment at rates comparable to the active stream. Not only does passage development occur under flood conditions but also in some active aquifers constant limestone dissolution may be occurring in a downwards direction, beneath the non-carbonate sediment. Keep in mind, Charon's Cascade was the first place that was chosen for this study, and it may not be representative of all river passages. Similar studies conducted within other karst aquifers may yeild different results. I recommend that a similar study be attempted within the Hawkins/Logsdon River system at Mammoth Cave, Kentucky to determine if similar results can be obtained in other areas.

An area of research that has received little attention within cave environments is the activity of microbes and its ability to decompose organic matter, increasing the carbon dioxide levels within the sediment. It was assumed that the elevated Pco_2 found within the sediment was a result of microbial decomposition of organic matter. Further research is needed to determine (1) if microbial decomposition of organic matter is responsible for the elevated Pco_2 levels with in the sediment, (2) identification of the types of micros within the sediment, (3) the specific source of the nutrients that the micros use for decomposition, and (4) what effects do the elevated Pco_2 levels with the sediment have on the global carbon cycle?

Also, further research is needed in the area of sediment transport and the effects of abrasion by clastic sediment on conduit enlargement. Once more research is completed on how the clastic sediment impacts limestone dissolution, a more accurate

rate equation for dissolution may be developed. Knowing how the clastic sediment in caves impacts passage development may be crucial for understanding both the rates and geometries of conduit evolution within karst aquifers, particularly the Mammoth Cave karst aquifer.

REFERENCES

Allison, J. D., D.S. Brown and K. J. Novo-Gradac, 1991, *MINTEQA2/PRODEFA, A Geochemical Assessment Model for Environmental Systems:* Version 3.0 User's Manual. Washington, D.C.: U.S. Environmental Protection Agency.

Anbeek, C., 1979, Surface roughness of mineral and implication for dissolution studies, *Geochim. Cosmochim. Acta,* vol. 56, pp. 1461-1469.

Anthony, D. M., 1998, *Seasonal Effects on the Geochemical Evolution of the Logsdon River, Mammoth Cave, Kentucky,* M.S. Thesis, geography Western Kentucky University.

Berner, R. A., 1980, *Early diagenesis: A Theoretical Approac,* Princeton, N.J., Princeton University Press, 241 p.

Berner, R. A. and J. W. Morse, 1974, Dissolution kinetics of calcium carbonate in sea water IV. Theory of calcite dissolution, *Amer. J. of Sci.,* vol. 274, pp. 108-134.

Brady, N. C., 1990, *The Nature and Properties of Soils*, New York, Macmillan Publishing Company, 621 p.

Boudreau, B. P., 1987, A steady state diagenetic model for dissolved carbonate species and pH in the porewaters of oxic and suboxic sediments, *Geochim. Cosmochim. Acta,* vol. 51, pp. 1985-1996.

Bouwer, H., 1978, *Groundwater Hydrology*, McGraw-Hill Series in Water Resource and Environmental Engineering, 356. p.

Brown, R. F. and T. W. Lambert, 1963, *Reconnaissance of Ground Water Resources in the Mississippian Plateau Region, Kentucky*, U.S. Geol. Survey Water-Supply paper 1603, 58 p.

Curl, R. L., 1965, Solution kinetics of calcite, *Proc., 4th Internat., Congress Speleol.*, (Ljubljana, Slovenia), vol. 3, pp. 61-66.

Cushman, R.V., R.A Krieger and J.A McCabe, 1965, Present and future water supply for Mammoth Cave National Park, Kentucky, pp. 601-647.

Davies, W. E. and E. C. Chao, 1959, *Report on Sediments in Mammoth Cave, Kentucky*. administrative report, 117 p. (Unpublished; copy held by Natl. Park Service at Mammoth Cave and by Geology Library at University of Texas at Austin).

Deike, G. H. III, 1967, *The Development of Caverns of the Mammoth Cave Region*, Ph.D Dissertation, The Pennsylvania State University, 235 p.

Dreybrodt, W., 1981, Kinetics of dissolution of calcite and its application to karstification, *Chem. Geol.*, vol. 31, pp. 245-269.

Dreybrodt, W., 1987, The kinetics of calcite dissolution and its consequences to karst evolution from the initial to the mature state, *Nat. Speleol. Soc. Bull.*, vol. 49, pp. 31-49.

Dreybrodt, W., 1988, *Processes in Karst Systems*, New York: Springer-Verlag, 288 p.

Dreybrodt, W., 1989, Karst development in its inital state: A model of speleogenesis, in: *Proceedings of the 10th International Congress of Speleology, Budapest,* Kosa, A. (Editor), vol. 1, pp. 174-176.

Dreybrodt, W., 1990, The role of dissolution kinetics in the development of karst aquifer in limestone: A model simulation of karst evolution, *Jour. Geol.*, vol. 98, pp. 639-655.

Dreybrodt, W., 1992, Dissolution kinetics of natural calcite minerals in CO_2-water systems approaching calcite equilibrium, *Chem. Geol.*, vol. 100, pp. 129-145.

Drever, J. I., 1997, *The Geochemistry of Natural Water*, Upper Saddle River, New Jersey Simon and Schuster, 436 p.

Fetter, C. W., 1992, *Applied Hydrogeology*, New York, Macmillan Publishing Company, 592 p.

Ford, D. C. and R. O. Ewers, 1978, The development of limestone cave systems in the dimensions of length and breadth, *Canada. J. Earth Sci.*, vol 15, pp. 1783-98.

Freeze, R. A., J. A. Cherry, 1979, *Groundwater*, Prentice-Hall, Engle-wood Cliffs, NJ. 604 p.

Greenberg, A. E., L. S. Clesceri, A. D. Eaton, and M. A. Franson (editors), 1992 *Standard Methods: For the Examination of Water and Waste Waters*. 18 th Edition, Washington D.C.. Amer Public Health Assoc., Amer Water Works Assoc., and Water Environment Federation.

Groves, C. G., 1991, KARSTSPEC, Unpublished BASIC computer program for calculations of equilibrium chemistry of karst waters.

Groves, C. G. and N. Crawford, 1990, Lithologic control of shallow karst groundwater flow on the Sinkhole Plain of Kentucky. *NSS Bulletin,* vol. 52, pp. 57-69.

Groves, C. G. and A. D. Howard, 1994a, Minimum hydrochemical conditions allowing limestone cave development, *Water Resources Res.,* vol. 30, pp. 186-191.

Groves, C. G. and A. D. Howard, 1994b, Early development of karst systems: 1. Preferential flowpath development under laminar flow, *Water Resources Res.,* vol. 30, pp. 2837-2846.

Groves, C. G. and J. Meiman, 1995a, The Hawkins River groundwater monitoring project, Mammoth Cave, Kentucky, *Geol. Soc. of Amer.*, vol. 27, No. 2, pp. 74.

Groves, C. G. and J. Meiman, 1995b, Storm water impacts on carbonate groundwater chemistry at the Hawkins River site, Mammoth Cave, Kentucky, *Geol. Soc. of Amer.*, vol. 27, No. 6 pp. 180.

Groves, C. G. and J. Meiman, 1996, Speleogenesis of Mammoth Cave: What are we learning at Hawkins River? in *Proceedings of the 5 th Mammoth Cave Science Symposium*, Mammoth Cave, Kentucky pp. 131-136.

Haynes, D. D., 1964, Geology of the Mammoth Cave Quadrangle, Kentucky, *U.S. Geol. Survey Map GQ-339,* Reston, VA.

Herman, J. S., and M.M. Lorah, 1987, CO_2 outgassing and calcite precipitation in Falling Spring Creek, Virginia, *Chem. Geol.,* vol. 62, pp. 251-262.

Hess, J.W., 1974, *Hydrochemical investigation of the central Kentucky karst aquifer system,* Ph.D Dissertation, Geology, The Pennsylvania State University, 218 p..

Hess, J. W., 1976, A review of the hydrogeology of the central Kentucky karst, *Water Resources Center, Desert Research Institute,* vol. 38, No. 4, October 1976.

Hess, J. W., S. G. Wells, J. F Quinlan, and W. B. White, 1989, Hydrogeology of the south-central Kentucky Karst, in *Karst Hydrology: Concepts from the Mammoth Cave Area*, White, W. and E. White, (editors) Van Nostrand Reinhold, New York, pp. 15-64.

Hess, J. W and W. B. White, 1989, Water budget and physical hydrology, in *Karst Hydrology: Concepts from the Mammoth Cave Area*, White, W and E. White, (editors) Van Nostrand Reinhold, New York, pp. 105-126.

Hess, J. W. and W. B. White, 1993, Groundwater geochemistry of the carbonate karst aquifer, south-central Kentucky, U.S.A., *Applied Geochemistry,* vol. 8, pp. 189-204.

Howard, A. D., 1968, Stratigraphic and structural controls on landforms development in the central Kentucky karst, *National Speleological Society Bulletin,* vol. 30, pp.95-114.

Howard, A. D. and C. G. Groves, 1995, Early development of karst systems; 2, turbulent flow, *Water Resources Res.*, vol. 31, pp. 19-26.

Incropera, F. P and D. P De Witt, 1985, *Fundamentals of Heat and Mass Transfer,* New York, John Wiley & Sons, 802 p.

Keir, R. S., 1982, Dissolution of calcite in the deep sea: Theoretical prediction for the case of uniform size particle settling into a well mixed sediment, *Amer. J. Sci.*, pp. 193-265.

Klute, A. (editor), 1985, *Methods of Soils Analysis Part 1 Physical and Mineralogical Methods*, Madison, Wisconsin, Amer. Soc. of Agronomy, SSSA Book Series 5, 1188 p.

Langmuir, D., 1971, The geochemistry of some carbonate groundwaters in central Pennsylvania, *Geochim. Cosmochim. Acta,* vol. 35, pp. 1023-1045.

Liu, C. and J. B. Evett, 1990, *Soil Properties: Testing, Measurement, and Evaluation*, Prentice-Hall, Englewood Cliffs, New Jersey, 375 p.

Meiman, J. and M. Ryan, 1993, The Echo River-Turnhole bend overflow route, *CRF Newsletter,* vol.1, pp. 15-18.

Miotke, F. D., 1975, Der Karst in zentralen Kentucky bei Mammoth Cave, *Jakrb. Geograph. Gesell. Hannover* 1973, pp.1-360.

Morse, J. W., 1983, The kinetics of calcium carbonate dissolution and precipitation, in: *Carbonates: Mineralogy and Chemistry,* A. Reeder (editor) Mineral Soc. Amer., vol. 11, pp. 274-264.

Murray, J. W., S. Emerson, and R. Jahnke, 1980, Carbonate saturation and the effect of pressure on the alkalinity of interstitial water from the Guatemala Basin, *Geochim. Cosochim. Acta,* vol. 44, pp. 963-972.

Palmer, A. N., 1981b, *A Geological Guide to Mammoth Cave National Park*, Teaneck, New Jersey: Zephyrus Press, 210. p.

Palmer, A. N., M.V. Palmer, and W. B. White, 1981a, *A Guide to the Historic Section of Mammoth Cave*, Bowling Green, Ky.: 8th International Congress of Speleology, 59 p.

Palmer, A. N., 1984, Geomorphic interpretation of karst features, In *Groundwater as a Geomorphic Agent*, R. G. LaFleur, (editor) (Allen and Unwin, London), pp. 173-209.

Palmer, A. N., 1989, Geomorphic history of the Mammoth Cave System: *in Karst Hydrology: Concepts from the Mammoth Cave Area*, White, W and E. White, (editors) Van Nostrand Reinhold, pp. 317-331.

Palmer, A. N., 1991, The origin and morphology of limestone caves, *Geol. Soc. Amer. Bull.* vol., 103, pp. 1-21.

Plummer, L. N., and T. M. L. Wigley, 1976, WATEQF-A FORTRAN IV version of WATEQ, a computer program for calculations of chemical equilibria in natural waters, *U.S. Geol. Surv. Water Resources Investigation*, pp. 76-113.

Plummer, L. N., T. M. L. Wigley, and D. L. Parkhurst, 1978, The kinetics of calcite dissolution in CO_2- water systems at 5 to 60^0 and 0.0 to 1.0 atm CO_2, *Amer. J. of Sci.* vol. 278, pp. 179-216.

Plummer, L. N., T M. L. Wigley, and D. L. Parkhurst, 1979, Critical review of the kinetics of calcite dissolution and precipitation, in *Chemical Modeling in Aqueous Systems*, E. A. Jeanne, (editor) Amer. Chem. Soc. Symp. Series 93, pp. 537-573.

Pohl, E. R., 1970, Upper Mississippian deposits of south-central Kentucky, *Kentucky Acad. Sci. Trans.*, vol. 1, pp. 1-15

Quinlan, J. F., 1970, Central Kentucky karst, *Études et Travaux de Méditerranée*, vol. 7 pp. 235-253.

Quinlan, J. F and R. Rowe, 1978, Hydrology and water quality in the central Kentucky karst: *Water Resources Institute*, University of Kentucky, Research, Report 109, 42 p.

Quinlan, J. F., and R. O. Ewers, 1989, Subsurface drainage in the Mammoth Cave Area: in *Karst Hydrology: Concept From the Mammoth Cave Area*, White, W. and E. White, (editors) Van Nostrand Reinhold, pp. 65-103.

Quinlan, J. F. and J. A. Ray, 1989, *Groundwater basins in the Mammoth Cave region, Kentucky*, Friends of Karst, Occasional Publication No.1, map.

Rauch, H. W. and W B. White, 1977, Dissolution kinetics of carbonate rock; 1, Effects of lithology on dissolution rates. *Amer. Geophysical Union, Washington, D.C.*, Water Resource Research vol. 13, No. 2, pp 381-394.

Renault, P., 1970, *The Formation of Caves,* Presses Univeritaires de France, Paris, France 127 p.

Sayles, F L., 1985, $CaCO_3$, Solubility in marine sediments: Evidence for equilibrium and non-equilibrium behaviour, *Geochim. Cosmochim. Acta,* vol. 49, pp. 877-888.

Shuster, E. T. and W. B. White, 1971, Seasonal fluctuations in the chemistry of limestone springs: A possible means for characterizing carbonate aquifers, *J. Hydrology* vol. 14, pp. 93-128.

Sherry M. B., 1993, *Modeling Steady State Groundwater and Surface Water Interaction*, Ph.D. Dissertation, Geology, Indiana University, 83 p.

Sjöberg, E. L., 1978, Kinetics and mechanisms of calcite dissolution in aqueous solution at low temperature, *Stockholm, Contrib. Geol.*, vol. 32, pp. 1-92.

Stumm, W and J. J. Morgan, 1981, *Aquatic Chemistry: An Introduction Emphasizing Chemical Equilibria in Natural Waters*, New York: John Wiley, 780 p.

Suarez, D. L., 1983, Calcite supersaturation and precipitation kinetics in the lower Colorado River, All American-Canal and East Highland Canal, *Water Resour. Res.*, vol. 19, pp. 653-661.

Trudgill, S. T., 1975, Measurement of erosional weight loss of rock tablets, *Brit. Geomorph. Res. Group Tech. Bull.* vol.17, pp 13-19.

Truesdell, A. H. and B. F. Jones, 1974, WATEQ: A computer program for calculating chemical equilibria of natural waters, *J. Res. U.S. Geol. Surv.*, vol. 2, pp. 233-274.

Walters, G. L. (editor), 1991, *Water Analysis Handbook; Photometric Procedures, Titration Procedures, Microbiological Procedures and Chemical Procedures Explained.* Hach Inc 712 p.

White, W. B., 1988, *Geomorphology and Hydrology of Karst Terrains*, New York: Oxford University Press, 464 p.

White, W B., 1989, Introduction to the karst hydrology of the Mammoth cave area: *in Karst Hydrology Concepts from the Mammoth Cave Area*, White, W. and E. White (editor), Van Nostrand Reinhold, pp. 1-14.

White, W. B. and G. H. Deike, 1989, Hydraulic geometry of cave passages: in *Karst Hydrology: Concepts from the Mammoth Cave Area*, White, W. and E. White, (editor), Van Nostrand Reinhold, New York, pp. 223-258.

White, E. L. and W. B. White, 1968, Dynamics of sediment transport in limestone caves, *Nat. Spel. Soc. Bull.*, vol. 30, pp. 115-129.

Wollast, R., 1990, Rate and mechanism of dissolution of carbonates in the system $CaCO_3$-$MgCO_3$, *Aquatic Chemical Kinetics: Reaction Rates of Processes in Natural Water*, New York: Wiley, pp. 431- 445.

APPENDIX A:

Chemistry of the water samples

A1. Constituents measured in the active stream at Charon's Cascade.

Date	pH	H^+ activity	t (°C)	spC (µs)	Ca^{2+} (mg/ L)	Mg^{2+} (mg/ L)	HCO_3 (mg/L)
3/28/98	7.69	$2.0x10^{-8}$	12.7	215	46		67
4/04/98	7.82	$1.5x10^{-8}$	12.1	207	42		62
4/06/98	7.84	$1.4x10^{-8}$	12.4	209	49	3.2	54
4/12/98	7.80	$1.6x10^{-8}$	12.3	210	37	3.2	58
5/17/98	7.65	$2.2x10^{-8}$	12.8	216	35	3.0	64
Mean	7.76	$1.7x10^{-8}$	12.5	211	42	3.1	61
SD	0.08	$3.5x10^{-9}$	0.35	3.9	5.9	0.1	4.9

A2. Constituents measured at a depth of 15 cm at Charon's Cascade.

Date	pH	H^+ activity	t (°C)	spC (µs)	Ca^{2+} (mg/ L)	Mg^{2+} (mg/ L)	HCO_3 (mg/L)
3/28/98	7.03	$9.3x10^{-8}$	11.9	336	60		142
4/04/98	7.09	$8.1x10^{-8}$	12.0	333	51		133
4/06/98	7.02	$9.5x10^{-8}$	12.1	345	59	8.3	146
4/12/98	7.09	$8.1x10^{-8}$	11.9	324	56	8.8	154
5/17/98	7.08	$8.3x10^{-8}$	13.0	323	53	7.2	134
Mean	7.06	$8.7x10^{-7}$	12.1	332	56	8.1	142
SD	0.03	$6.8x10^{-9}$	0.47	9.6	3.8	0.82	8.7

A3. Constituents measured at a depth of 30 cm at Charon's Cascade.

Date	pH	H^+ activity	t (°C)	spC (µs)	Ca^{2+} (mg/ L)	Mg^{2+} (mg/ L)	HCO_3 (mg/L)
3/28/98	6.97	$1.1x10^{-7}$	11.7	327	58		140
4/04/98	7.03	$9.3x10^{-8}$	11.8	376	59		110
4/06/98	7.02	$9.5x10^{-8}$	12.1	330	59	8.2	112
4/12/98	7.09	$8.1x10^{-8}$	11.6	313	58	7.0	104
5/17/98	7.09	$8.1x10^{-8}$	12.8	264	47	6.1	110
Mean	7.03	$9.2x10^{-8}$	12.0	322	56	7.1	115
SD	0.05	$1.2x10^{-8}$	0.48	40	5.2	1.1	14

A4. Constituents measured at a depth of 60 cm at Charon's Cascade.

Date	pH	H^+ activity	t (°C)	spC (µs)	Ca^{2+} mg/ L	Mg^{2+} mg/ L	HCO_3 mg/L
3/28/98	6.95	$1.1x10^{-7}$	11.6	332	58		143
4/04/98	6.94	$1.2x10^{-7}$	11.6	313	61		132
4/06/98	6.92	$1.2x10^{-7}$	11.9	325	51	8.1	112
4/12/98	7.04	$9.1x10^{-8}$	11.6	323	56	7.3	140
5/17/98	7.08	$8.3x10^{-8}$	12.8	348	58	6.7	152
Mean	6.98	$1.2x10^{-7}$	11.9	326	57	7.4	136
SD	0.07	$2.1x10^{-8}$	0.52	9.5	3.7	0.7	15

A5. Constituents measured at a depth of 90 cm at Charon's Cascade.

Date	pH	H^+ activity	t (°C)	spC (µs)	Ca^{2+} (mg/ L)	Mg^{2+} (mg/ L)	HCO_3 (mg/L)
3/28/98	6.95	$1.1x10^{-7}$	11.6	328	56		132
4/04/98	6.90	$1.3x10^{-7}$	11.6	325	61		134
4/06/98	6.92	$1.2x10^{-7}$	11.9	335	56	9.5	144
4/12/98	6.99	$1.0x10^{-7}$	11.4	373	53	5.2	104
5/17/98	7.06	$8.7x10^{-8}$	12.6	406	53	6.6	112
Mean	6.96	$1.1x10^{-7}$	11.8	353	56	7.1	125
SD	0.06	$3.8x10^{-7}$	0.47	35	3.3	2.2	15

APPENDIX B:

Saturation indices and Pco_2 concentrations at Charon's Cascade and collection sample dates

B1. Saturation indices and Pco_2 pressures at Charon's Cascade, Mammoth Cave.

3/28/98	SI calcite	SI dolomite	Pco_2 (atm)	Pco_2 ÷ atm background
stream	-0.375		$1.2x10^{-3}$	3.4
15 cm	-0.728		$8.9x10^{-3}$	25.4
30 cm	-0.817		$9.8x10^{-3}$	28.0
60 cm	-0.834		0.0104	29.7
90 cm	-0.879		$9.6x10^{-3}$	27.4

B2. Saturation indices and Pco_2 pressures at Charon's Cascade, Mammoth Cave.

4/4/98	SI calcite	SI dolomite	Pco_2 (atm)	Pco_2 ÷ atm background
stream	-0.319		$8.1x10^{-4}$	2.3
15 cm	-0.718		$7.9x10^{-3}$	22.7
30 cm	-0.893		$6.9x10^{-3}$	19.9
60 cm	-0.859		$9.8x10^{-3}$	27.9
90 cm	-0.902		0.0106	30.3

B3. Saturation indices and Pco_2 pressures at Charon's Cascade, Mammoth Cave.

4/6/98	SI calcite	SI dolomite	Pco_2 (atm)	Pco_2 ÷ atm background
stream	-0.392	-1.71	$6.7x10^{-4}$	1.9
15 cm	-0.734	-2.17	$9.4x10^{-3}$	26.8
30 cm	-0.844	-2.39	$7.2x10^{-3}$	20.6
60 cm	-0.991	-2.63	$8.2x10^{-3}$	23.4
90 cm	-0.888	-2.39	$1.1x10^{-2}$	31.5

B4. Saturation indices and Pco_2 pressures at Charon's Cascade, Mammoth Cave.

4/12/98	SI calcite	SI dolomite	Pco_2 (atm)	Pco_2 ÷ atm background
surface	-0.419	-1.75	$7.9x10^{-4}$	2.3
15 cm	-0.656	-1.95	$8.7x10^{-3}$	24.6
30 cm	-0.809	-2.37	$5.8x10^{-3}$	16.6
60 cm	-0.757	-2.24	$8.6x10^{-3}$	24.5
90 cm	-0.963	-2.77	$7.0x10^{-3}$	20.0

B5. Saturation indices and Pco_2 pressures at Charon's Cascade, Mammoth Cave.

5/17/98	SI calcite	SI dolomite	Pco_2 (atm)	Pco_2 ÷ atm background
surface	-0.538	-1.99	$1.2x10^{-3}$	3.4
15 cm	-0.726	-2.17	$7.8x10^{-3}$	22.4
30 cm	-0.850	-2.43	$6.3x10^{-3}$	17.9
60 cm	-0.643	-2.07	$8.8x10^{-3}$	25.2
90 cm	-0.831	-2.41	$6.7x10^{-3}$	19.3

APPENDIX C:

Purity of the limestone that was used to measure actual limestone dissolution rates within the sediment

Purity of limestone samples	total weight	tare weight	limestone weight	insoluble weight	limestone (wt ÷ insoluble)	purity (final wt - 1.0) x 100
sample 1	4.414	1.019	3.396	.1124	0.0331	96.7 %
sample 2	4.128	1.019	3.109	.1022	0.0329	96.7 %
sample 3	4.400	1.019	3.381	.1176	0.0348	96.5 %
sample 4	4.437	1.019	3.418	.091	0.0266	97.3 %

APPENDIX D:

Sediment core profiles from the River Styx and from the base of Charon's Cascade

Sediment core samples were collected from the River Styx and Charon's Cascade. All sediment profiles are described from the uppermost sampling depth to the bottom, and all classifications are based on Munsell color charts. When facing the River Styx standing under Charon's Cascade, sample one was taken from the left, sample two from the center, and sample three from the right from the base of the water fall. Sediment core four was taken from the upper end of the River Styx (Figure 12 and 14).

D1. Core sample 1 Charon's Cascade.

Length	Texture classification	Munsell Color Chart Classification
0.0 - 10.2 cm	sandy loam	dark brown 7.5 YR 4.2
10.2 - 34.2 cm	sand	light to dark brown 7.5 YR 5/4
32.2 - 44.2 cm	loam	gray brown 2.5 Y 5/2
44.2 - 50.8 cm	sand	pale brown 10 YR 5/2

D2. Core sample 2 Charon's Cascade

Length	Texture Classification	Munsell Color Chart Classification
0.0 - 16.5 cm	loam	brown 7.5 YR 4/4
16.5 - 22.9 cm	sand	pale brown 10 YR 6/3
22.9 - 38.1 cm	silt loam	dark brown 7.5 YR 4/4
38.1 - 58.4 cm	sandy loam	dark gray brown 2.5 Y 4/2
58.4 - 66.0 cm	silt loam	gray brown 2.5 Y 5/2
66.0 - 68.6 cm	loamy sand	reddish brown 5 YR 4/3

D3. Core sample 3 Charon's Cascade

Length	Texture Classification	Munsell Color Chart Classification
0.0 - 12.1 cm	sand	reddish brown 5 YR 5/4
12.1 - 17.8 cm	sand	the top part is black 5 YR 2/1 and the bottom is yellowish re 5 YR 5/8 from manganese oxide stains
17.8 - 47.0 cm	silt loam	gray 5 Y 5/1
47.0 - 53.4 cm	sandy loam	tan to grayish brown 10 YR 5/2
53.4 - 68.7 cm	sandy loam	gray 5 Y 5/1
68.7 - 76.3 cm	silty clay loam	a mix of light brownish gray 10 YR to a olive gray 5 Y 5/2
76.3 - 85.0 cm	sandy loam	grayish brown 10 YR 5/2

D4. Core sample 4 upper end of River Styx

Length	Texture Classification	Munsell Color Chart Classification
0.0 - 34.9 cm	sandy loam	reddish brown, 5 YR 4/4
34.9 - 35.5 cm	loamy sand	yellowish red, 5 YR 5/8 manganese oxide stain
35.5 - 81.2 cm	sandy loam	reddish brown, 5 YR 4/4
81.2 - 88.9 cm	sandy loam	dark yellowish brown, 10 YR 4/4

APPENDIX E:

Weight of the limestone tablets before they were placed within the sediment

Sample number	Heated/Vacuumed and Weighed limestone blocks in g.	Unheated limestone blocks in g.	Difference between Heated and Unheated limestone blocks in g.
1.	3.7257	3.7308	0.0051
2.	5.5635	5.5726	0.0091
3.	4.8448	4.8502	0.0054
4.	4.8940	4.9027	0.0087
5.	6.0977	6.1073	0.0096
6.	3.9414	3.9455	0.0041
7	5.5946	5.6048	0.0102
8.	4.7134	4.7180	0.0046
9.	5 4129	5.4201	0.0072
10.	4.5979	4.6055	0.0076
11.	5.4566	5.4647	0.0081
12.	4.7645	4.7695	0.0050
13.	4.9644	4.9714	0.0070
14.	5.1667	5.1758	0.0091
15.	5.5644	5.5717	0.0073
16.	5.7385	5.7459	0.0074
17.	7.2074	7.2190	0.0116
18.	7.1805	7.1916	0.0111
19.	5.5574	5.5657	0.0083
20.	7.5521	7.5646	0.0125
21.	4.8113	4.8194	0.0081
22.	4.8878	4.8947	0.0069

23.	5.4465	5.4541	0.0076
24.	5.5729	5.5806	0.0077
25.	4.6287	4.6368	0.0081
26.	4.2173	4.2266	0.0093
27.	4.4941	4.5000	0.0059
28.	5.5646	5.5730	0.0084
29.	4.4839	4.4913	0.0074
30	4.0988	4.1043	0.0055
31.	3.4941	3.5000	0.0059
32.	4.5428	4.5502	0.0074
33.	4.6539	4.6592	0.0053
34.	4.0604	4.0654	0.0050
35.	4.4357	4.4428	0.0071
36.	4.1070	4.1136	0.0066
37.	3.3017	3.3063	0.0046
38.	3.3737	3.3786	0.0049
39.	3.2374	3.2426	0.0052
40.	3.0611	3.0674	0.0063
41.	3.0236	3.0294	0.0058
42.	2.9485	2.9556	0.0071
43.	3.0151	3.0206	0.0051

	Mean Weight Difference 0.0071 g	Standard Deviation 0.0022 g

APPENDIX F

Limestone tablets surface area

Stone Number	Height in cm	Length in cm	Width in cm	Surface area cm^2
1	0.3556	2.0320	1.5748	9.1614
2	0.3556	2.5908	2.1336	14.6113
3	0.4064	2.2860	1.8288	11.9536
4	0.4064	2.3368	1.7780	11.6539
5	0.4572	2.3876	2.0828	14.0335
6	0.4572	2.4892	2.1844	14.1987
7	0.4572	2.2860	2.0828	13.5174
8	0.3556	2.3368	1.8796	11.7832
9	0.4064	2.5400	2.0828	14.3380
10	0.4572	2.2352	1.7780	11.6180
11	0.4572	2.2860	2.0828	13.5174
12	0.4064	2.2352	2.0320	12.5522
13	0.4064	2.2860	1.8796	11.9793
14	0.4064	2.3876	2.0828	13.5793
15	0.4572	2.2860	2.0828	13.5174
16	0.4064	2.5400	2.1336	14.6374
17	0.4572	2.4892	2.4384	16.6451
18	0.4572	2.4892	2.3876	16.3458
19	0.4572	2.3368	2.0828	13.7755
20	0.4572	2.8956	2.2352	17.6361
21	0.3556	2.5400	1.8796	12.6916
22	0.4572	2.3368	1.5240	10.6529
23	0.4572	2.3368	1.9812	13.2077
24	0.4572	2.3368	2.0320	13.4916

25	0.4572	2.0320	1.8288	10.9626
26	0.3556	2.5400	1.7780	12.1032
27	0.3556	2.1336	2.0320	11.6335
28	0.4572	2.4384	1.8796	13.1148
29	0.4572	2.2860	1.6256	11.0090
30	0.4572	1.9812	1.7780	10.4826
31	0.3556	2.0320	1.7780	9.9355
32	0.4572	2.0320	1.9304	11.4684
33	0.4572	2.3876	1.6256	11.4322
34	0.4064	2.0828	1.8796	11.0503
35	0.4572	2.2860	1.6256	11.0090
36	0.4572	2.0828	1.5240	9.6464
37	0.3556	1.9304	1.6764	9.0374
38	0.3556	1.9304	1.7780	9.5019
39	0.3556	1.8288	1.7780	9.0684
40	0.4572	1.8288	1.4732	8.4077
41	0.4572	1.7780	1.4732	8.2116
42	0.3556	1.9304	1.5748	8.5729
43	0.4064	1.8796	1.6256	8.9600

APPENDIX G:

Limestone tablet placement on individual angle brace

G1. There were five levels on each rod with two limestone tablets per level.

sample depth	rod 1	rod 1	rod 2	rod 2	rod 3	rod 3	rod 4	rod 4
stream		36	38	39			42	43
15 cm	30	25	28	34	1	37	13	20
30 cm	8	9	16	17	6	24	32	33
60 cm	31	22	5	7	12	4	19	18
90 cm	14	11	10	27	2	29	35	3

APPENDIX H:

Individual limestone tablet weight loss in grams

H1. There were five levels on each rod with two limestone tablets per level.

sample depth	rod 1	rod 1	rod 2	rod 2	rod 3	rod 3	rod 4	rod 4
surface		0.0050	0.0065	0.0108			0.0041	0.0032
15 cm	0.0025	0.0017	0.0056	0.0044	0.0051	0.0048	0.0031	0.0061
30 cm	0.0011	0.002	0.0050	0.0110	0.0027	0.0025	0.0009	0.0014
60 cm	0.0025	0.0043	0.0052	0.0058	0.0060	0.0017	0.0047	0.0029
90 cm	0.0025	0.0030	0.0026	0.0027	0.0006	0.0022	0.0021	0.0003

APPENDIX I:

Hydrometer analysis

I. Hydrometer analysis by depth from the push core sample collected from Charon's Cascade.

	0 to 30 cm deep		30 to 60 cm deep		60 to 90 cm deep	
Time	hydrometer depth	percent silt and clay	hydrometer depth	percent silt and clay	hydrometer depth	percent silt and clay
30 sec	8	20.0	11	27.5	25	62.5
1 min	7	17.5	9	22.5	24	60.0
3 min	5	12.5	8	20.0	21	52.5
10 min	4	10.0	6	15.0	17	42.5
30 min	3	7.5	4	10.0	11	27.5
60 min	2	5.0	4	10.0	10	25.0
90 min	2	5.0	3	7.5	9	22.5
120 min	2	5.0	3	7.5	8	20.0
1440 min	2	5.0	3	7.5	7	17.5

APPENDIX J:

Silt and clay size particles determined from the Hydrometer tests

Particle sizes were determined by the following equation:

$X = \theta t^{-1/2}$
$\theta = (18\eta h'/[g (p_s - p_1)])^{1/2}$

Where,
η = 0.8345×10^{-3} kg m^{-1} s^{-1}
h' = -0.164 R + 16.3
R = the uncorrected hydrometer reading
g = 9.81 m/s^2
p_s = 2.65 g $/cm^3$
p_1 = solution density at temperature t, g/ml

J. Particles sizes were determined by depth from the push core sample, and the results were plotted on a cumulative frequency diagram (Appendix L)

Time	0 - 30 cm particle sizes	30 - 60 cm particle sizes	60 - 90 cm particle sizes
30 sec	0.017	0.016	0.014
1 min	0.012	0.012	0.011
3 min	0.007	0.007	0.006
10 min	0.004	0.004	0.003
30 min	0.0022	0.0022	0.002
60 min	0.0016	0.0015	0.0015
90 min	0.0013	0.0013	0.0012
120 min	0.0011	0.0011	0.0011
1440 min	0.0003	0.0003	0.0003

APPENDIX K:

Mechanical sieve analysis of the sediment collected from a push core sample at the base of Charon's Cascade

K1. Mechanical sieve analysis of the sediment collected from 0 to 30 cm

Sample 1	starting weight 40 grams			
mesh (U.S.)	raw weight	weight %	cumulative weight	cumulative %
10	0	0	0	0
18	0	0	0	0
35	0.114	0.2	0.1	0.2
60	0.514	1.28	0.6	1.48
120	9.256	23.14	9.8	24.62
230	6.67	16.7	16.5	41.32
pan	23.44	58.6	39.9	100

K1. Mechanical sieve analysis of the sediment collected from 30 to 60 cm.

Sample 2	starting weight 40 grams			
mesh (U.S.)	raw weight	weight %	cumulative weight	cumulative %
10	0	0	0	0
18	0.2	2.5	0.2	0.2
35	1.16	2.9	1.36	3.1
60	5.1	12.7	6.46	15.8
120	16.4	41	22.86	56.8
230	7.37	18.4	30.23	75
pan	9.7	24.4	39.9	100

K1. Mechanical sieve analysis of the sediment collected from 60 to 90 cm.

Sample 3	starting weight 40 grams			
mesh (U.S.)	raw weight	weight %	cumulative weight	cumulative %
10	0	0	0	0
18	0.036	0.1	.036	0.1
35	0.356	0.89	0.386	0.99
60	5.51	13.77	5.88	14.76
120	17.66	44	23.48	58.9
230	7.23	18	30.70	76.9
pan	9.20	23	39.9	100

APPENDIX L.

Cumulative frequency plots of the push core samples used for measuring the hydraulic conductivity

L1.Cumulative frequency plot of sediment sample from Charon's Cascade (0 - 31 cm).

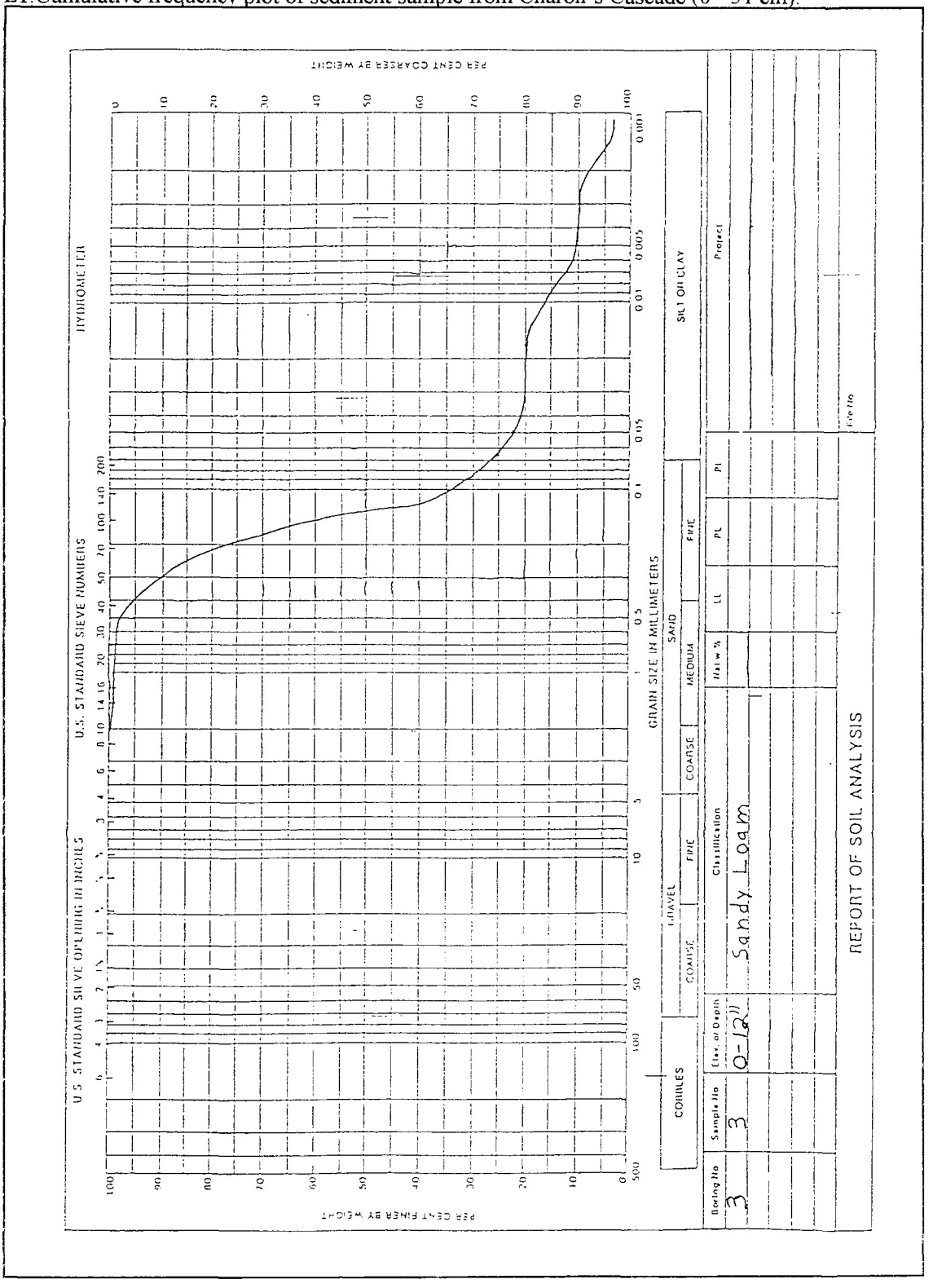

L2. Cumulative frequency plot of sediment sample from Charon's Cascade (31 - 61 cm).

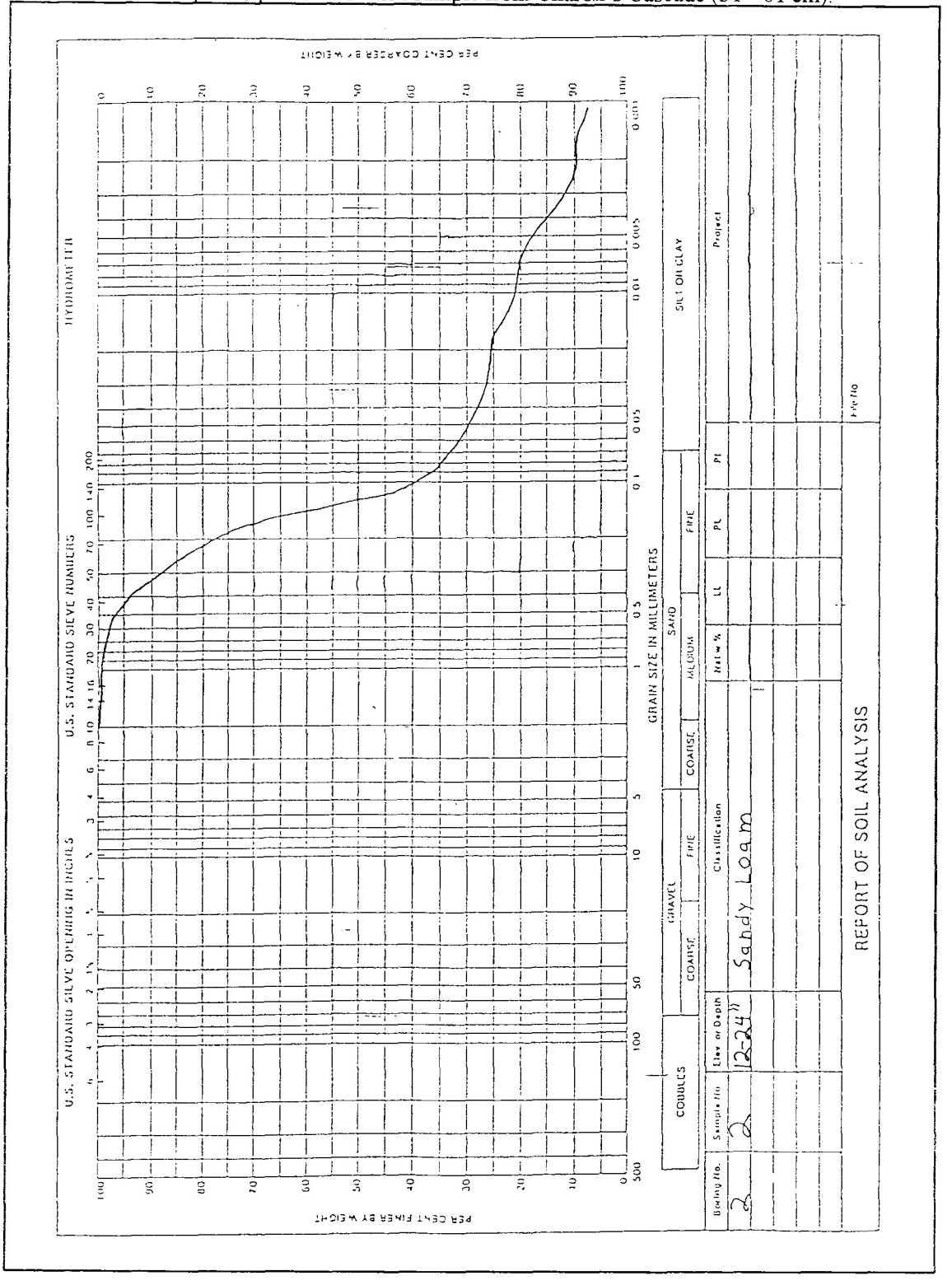

L3. Cumulative frequency plot of sediment sample from Charon's Cascade (61 - 91 cm).